Article

Synthesis and Characterization of Salts Containing the BrOF Anion; A Rare Example of a Bromine(VII) Species

John F. Lehmann, and Gary J. Schrobilgen

J. Am. Chem. Soc., **2005**, 127 (26), 9416-9427• DOI: 10.1021/ja0402607 • Publication Date (Web): 08 June 2005

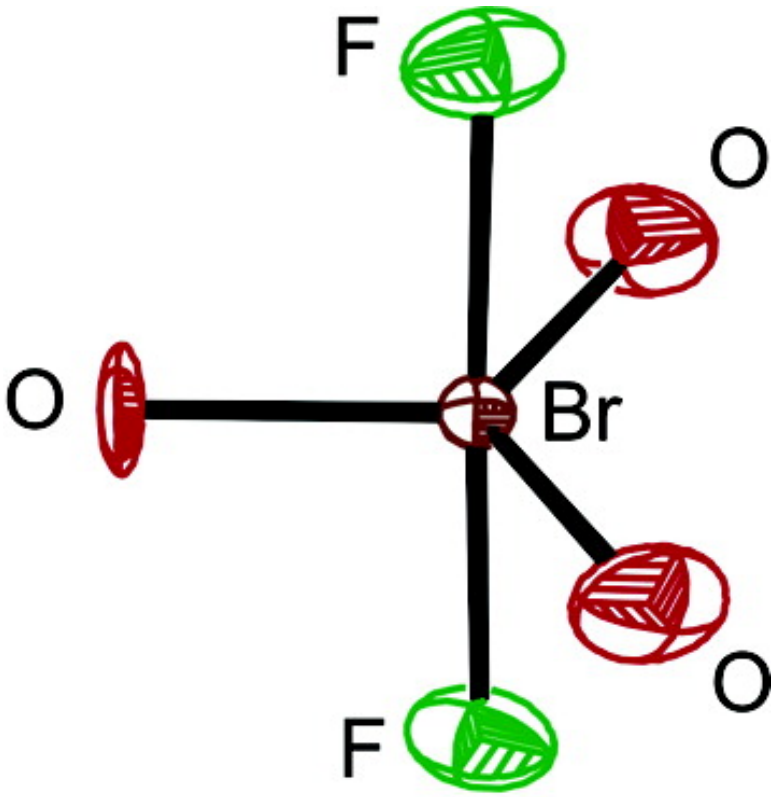

$BrO_3F_2^-$

J|A|C|S
ARTICLES
Published on Web 06/08/2005

Synthesis and Characterization of Salts Containing the $BrO_3F_2^-$ Anion; A Rare Example of a Bromine(VII) Species

John F. Lehmann and Gary J. Schrobilgen*

Contribution from the Department of Chemistry, McMaster University, Hamilton, Ontario, L8S 4M1, Canada

Received November 23, 2004; E-mail: schrobil@mcmaster.ca

Abstract: The $BrO_3F_2^-$ anion has been prepared by reaction of BrO_3F with the fluoride ion donors KF, RbF, CsF, $[N(CH_3)_4][F]$, and NOF. The $BrO_3F_2^-$ anion is only the fourth Br(VII) species to have been isolated in macroscopic quantities, and it is one of only three oxide fluorides that possess D_{3h} symmetry, the others being XeO_3F_2 and OsO_3F_2. The fluoride ion acceptor properties of BrO_3F contrast with those of ClO_3F, which does not react with the strong fluoride ion donor $[N(CH_3)_4][F]$ to form the analogous $ClO_3F_2^-$ salt. The single-crystal X-ray structures of $[NO]_2[BrO_3F_2][F]$ and $[N(CH_3)_4][BrO_3F_2]$ confirm the D_{3h} symmetry of the $BrO_3F_2^-$ anion and provide accurate Br−O (1.593(3)−1.610(6) Å) and Br−F (1.849(5)−1.827(4) Å) bond lengths. The salt, $[NO]_2[BrO_3F_2][F]$, is fully ordered, crystallizing in the monoclinic space group, *C*2/*c*, with $a = 9.892(3)$ Å, $b = 12.862(4)$ Å, $c = 10.141(4)$ Å, $\beta = 90.75(2)°$, $V = 12460(7)$ Å^3, $Z = 4$, and $R_1 = 0.0671$ at −173 °C, whereas $[N(CH_3)_4][BrO_3F_2]$ exhibits a 2-fold disorder of the anion, crystallizing in the tetragonal space group, *P*4/*nmm*, with $a = 8.5718(7)$ Å, $c = 5.8117(6)$ Å, $V = 427.02(7)$ Å^3, $Z = 2$, and $R_1 = 0.0314$ at −173 °C. The ^{19}F chemical shift of $[N(CH_3)_4][BrO_3F_2]$ in CH_3CN is 237.0 ppm and is more deshielded than those of the previously investigated Br(VII) species, BrO_3F and BrF_6^+. The vibrational frequencies of the $BrO_3F_2^-$ anion were determined by use of Raman and infrared spectroscopy and were assigned with the aid of electronic structure calculations and by analogy with the vibrational assignments reported for XeO_3F_2 and OsO_3F_2. The internal and symmetry force constants of $BrO_3F_2^-$ were determined by use of general valence force field and B-matrix methods, respectively, and are compared with those of XeO_3F_2, OsO_3F_2, and the unknown $ClO_3F_2^-$ anion. The instability of $ClO_3F_2^-$ relative to $BrO_3F_2^-$ has been investigated by electronic structure calculations and rationalized in terms of atomic charges, Mayer bond orders, and Mayer valencies, and the enthalpies of fluoride ion attachment to BrO_3F and ClO_3F.

Introduction

Prior to the present study, the only Br(VII) species that had been prepared in macroscopic quantities and characterized were BrO_3F,[1] salts of the BrF_6^+,[2,3] and BrO_4^-[4−7] (including $HBrO_4$[6,7]) ions.[8] The synthetic challenges associated with the syntheses of Br(VII) compounds are consistent with the general reluctance of late row four elements of the periodic table to attain their highest oxidation states.

The ability of main-group and transition-metal fluorides and oxide fluorides to accept or donate fluoride ions is well-known, providing routes to anionic and cationic derivatives of BrF_3 (BrF_2^+,[9,10] BrF_4^-[11]), BrF_5 (BrF_6^-,[12] BrF_4^+[13,14]), BrO_2F ($BrO_2F_2^-$,[15] BrO_2^+[16,17]), and $BrOF_3$ ($BrOF_4^-$,[18,19] $BrOF_2^+$[20,21]). Fluoride ion transfer reactions, however, have not been used to prepare new cations and anions derived from known Br(VII) species. Among Br(VII) species, BrF_6^+ and BrO_3F might be expected to accept fluoride ions leading to BrF_7 and $BrO_3F_2^-$ or to act as a fluoride ion donor leading to BrO_3^+. Although a high-temperature synthesis of BrF_7 has been reported,[22] the existence of BrF_7 was shown to be unlikely because the reaction of BrF_6^+ with NOF at −78 °C results in reduction to BrF_6^- with the evolution of F_2,[3] and because attempts to form BrF_7 by oxidation of BrF_5 with F_2 under photolytic conditions at −40 to −60 °C have also failed.[23] The fluoride ion donor properties of BrO_3F have

(1) Appelman, E. H. Studier, M. H. *J. Am. Chem. Soc.* **1969**, *91*, 4561.
(2) Gillespie, R. J.; Schrobilgen, G. J. *J. Chem. Soc., Chem. Commun.* **1974**, 90.
(3) Gillespie, R. J.; Schrobilgen, G. J. *Inorg. Chem.* **1974**, *13*, 1230.
(4) Brown, L. C.; Begun, G. M.; Boyd, G. E. *J. Am. Chem. Soc.* **1969**, *91*, 2250.
(5) Appelman, E. H. *J. Am. Chem. Soc.* **1968**, *90*, 1900.
(6) Appelman, E. H. *Inorg. Synth.* **1971**, *13*, 1.
(7) Appelman, E. H. *Inorg. Chem.* **1969**, *8*, 223.
(8) Isopropyl perbromate, $(CH_3)_2CHOBrO_3$, has been reported but is poorly characterized (Baum, K.; Beard, C. D.; Grakauskas, V. *J. Am. Chem. Soc.* **1975**, *97*, 267).
(9) Woolf, A. A.; Emeléus, H. J. *J. Chem. Soc.* **1949**, 2865.
(10) Brown, D. H.; Dixon, K. R.; Sharp, D. W. A. *Chem. Commun.* **1966**, 654.
(11) Siegel, S. *Acta Crystallogr.* **1956**, *9*, 493.
(12) Bougon, R.; Charpin, P.; Soriano, J. *C. R. Hebd. Séances Acad. Sci. Ser. C* **1971**, *272*, 565.
(13) Lind, M. D.; Christe, K. O. *Inorg. Chem.* **1972**, *11*, 608.
(14) Vij, A.; Tham, F. S.; Vij, V.; Wilson, W. W.; Christe, K. O. *Inorg. Chem.* **2002**, *41*, 6397.
(15) Gillespie, R. J.; Spekkens, P. H. *J. Chem. Soc., Dalton Trans.* **1977**, 1539.
(16) Jacob, E. *Angew. Chem., Int. Ed. Engl.* **1976**, *15*, 158; *Angew. Chem.* **1976**, *88*, 189.
(17) Spekkens, P. H. Ph.D. Thesis, McMaster University, Hamilton, Ontario, Canada, 1977; pp 87−104.
(18) Gillespie, R. J.; Spekkens, P. *J. Chem. Soc., Dalton Trans.* **1976**, 2391.
(19) Bougon, R.; Joubert, P.; Tantot, G. *J. Chem. Phys.* **1977**, *66*, 1562.
(20) Adelhelm, E.; Jacob, E. *Angew. Chem., Int. Ed. Engl.* **1977**, *16*, 461; *Angew. Chem.* **1977**, *89*, 476.
(21) Bougon, R.; Huy, T. B.; Charpin, P.; Gillespie, R. J.; Spekkens, P. H. *J. Chem. Soc., Dalton Trans.* **1979**, 6.
(22) Fogle, C. E.; Rewick, R. T. U.S. Patent 3615206, 1971.

10.1021/ja0402607 CCC: $30.25

been assessed in anhydrous HF solvent by monitoring solutions of BrO_3F and SbF_5 by Raman spectroscopy, and solutions of BrO_3F and AsF_5 by ^{19}F NMR spectroscopy.[24] The absence of vibrational frequency shifts or changes in the ^{19}F NMR chemical shift of BrO_3F in these studies indicates that interactions between the ligand atoms of BrO_3F and the Lewis acids are weak to negligible. Although the fluoride ion acceptor properties of BrO_3F have not been explicitly investigated, the observation that CsF and NO_2F do not behave as fluoride ion donors toward ClO_3F[25] has led to speculation that BrO_3F may also be a poor fluoride ion acceptor.[24] Recent theoretical calculations,[26] however, suggest that BrO_3F may react with strong fluoride ion donors such as $[N(CH_3)_4][F]$, so-called "naked fluoride".[27]

The VSEPR model of molecular geometry[28] predicts that the $BrO_3F_2^-$ and $ClO_3F_2^-$ anions should possess trigonal bipyramidal geometries (D_{3h} symmetry) in which the three oxygen atoms occupy the equatorial positions and the two fluorine atoms occupy the axial positions. Although the trigonal bipyramidal geometry is common among neutral, gas-phase, and anionic inorganic pentahalides,[29] the only trigonal bipyramidal EO_3F_2 species known are XeO_3F_2[30] and OsO_3F_2.[31,32] Moreover, OsO_3F_2 is a polymeric *cis*-fluorine bridged chain structure in the solid state,[33] but has been shown by vibrational spectroscopy to exist as a monomer having D_{3h} symmetry when isolated in a matrix.[31,32] The challenging synthesis of XeO_3F_2 by the reaction of XeO_4 with XeF_6 has yet to yield bulk quantities of pure XeO_3F_2, but ^{19}F NMR spectroscopy of SO_2ClF, HF, and BrF_5 solutions of XeO_3F_2,[34] and vibrational (Raman, IR) spectra of XeO_3F_2 isolated in Ar and Ne matrices[30] have confirmed the predicted D_{3h} geometry.[35] The geometric parameters of XeO_3F_2 and the OsO_3F_2 monomer have not been determined.

The present work investigates the fluoride ion acceptor behavior of BrO_3F toward a range of fluoride ion donors, with the view to synthesize salts of the $BrO_3F_2^-$ anion, thus providing a significant extension of Br(VII) chemistry and the first example of a trioxide difluoride anion. The study also reinvestigates the fluoride ion acceptor properties of ClO_3F.

Results and Discussion

Syntheses of $[M][BrO_3F_2]$ (M = K, Rb, Cs, $N(CH_3)_4$) and $[NO]_2[BrO_3F_2][F]$. The fluoride ion acceptor properties of BrO_3F were investigated by monitoring its reactions with NOF and MF by means of Raman spectroscopy. An initial attempt to synthesize $[Cs][BrO_3F_2]$ in anhydrous HF failed to provide Raman spectroscopic evidence for fluoride ion transfer to BrO_3F, suggesting that fluoride ion transfer to BrO_3F is thermodynamically less favorable than fluoride ion transfer to HF. Consequently, the use of HF as a solvent was abandoned for the remainder of these studies.

Although violent detonations occasionally occurred when BrO_3F was brought into contact with CH_3CN, the high first adiabatic ionization potential (13.59 eV),[36] favorable liquid range, and resistance to fluoride ion attack at low temperatures[37,38] make CH_3CN a useful solvent for the synthesis of anions derived from strong oxidative fluorinators.[39,40] The $N(CH_3)_4^+$, K^+, Rb^+, and Cs^+ salts of $BrO_3F_2^-$ were synthesized (eq 1) and handled in CH_3CN solvent for prolonged periods of time at low temperatures (<−30 °C) and at ambient temperatures for short periods of time.

$$MF + BrO_3F \rightarrow [M][BrO_3F_2]\ (M = K, Rb, Cs, N(CH_3)_4) \quad (1)$$

Raman spectroscopy was used to verify salt formation prior to solvent removal under dynamic vacuum at −40 °C. The reactivities of $[N(CH_3)_4][F]$ and CsF toward BrO_3F were similar, with $[N(CH_3)_4][BrO_3F_2]$ and $[Cs][BrO_3F_2]$ formation proceeding smoothly over a period of an hour at −40 to −48 °C. The low-temperature α-phase of $[Cs][BrO_3F_2]$ was isolated when the solution was maintained at or below −40 °C during reaction and removal of the solvent, whereas the high-temperature β-phase of $[Cs][BrO_3F_2]$ was isolated when the reaction and solvent removal were carried out at −35 °C. The β-phase of $[Cs][BrO_3F_2]$ may alternatively be obtained by allowing α-$[Cs][BrO_3F_2]$ to stand at 0 °C for 35 h in the absence of a solvent; however, the reverse process does not occur at temperatures as low as −78 °C over a period of 4 days. The reactions of KF and RbF with BrO_3F were slow at −40 °C when compared with the nearly instantaneous formation of $[N(CH_3)_4][BrO_3F_2]$ and α-$[Cs][BrO_3F_2]$ at or below this temperature, but proceeded rapidly at −30 to −35 °C. The slower reaction rates of KF and RbF at temperatures below −40 °C likely reflect their lower solubilities.

The double salt, $[NO]_2[BrO_3F_2][F]$, was prepared by the reaction of BrO_3F with neat NOF at −78 °C (eq 2) for 5 min followed by rapid removal (ca. 30 s) of excess NOF under dynamic vacuum at −78 °C.

$$2NOF + BrO_3F \rightarrow [NO]_2[BrO_3F_2][F] \quad (2)$$

The colorless product had a significant dissociation vapor pressure at −78 °C and was crystallized by allowing the solid to sublime under 1000 Torr of Ar over a period of several weeks at −78 °C. The Raman spectra of the initial and crystallized products were identical, and single-crystal X-ray diffraction was used to establish the product stoichiometry in eq 2.

Attempted Syntheses of $[N(CH_3)_4]_2[BrO_3F_3]$ and $[N(CH_3)_4][ClO_3F_2]$. The reaction of $[N(CH_3)_4)][BrO_3F_2]$ with a stoichiometric amount of $[N(CH_3)_4)][F]$ was attempted at 0 °C in CH_3CN solvent. Upon removal of the solvent at −40 °C, the Raman spectrum of the remaining solid showed that it was a

(23) Pilipovich, D.; Rogers, H. H.; Wilson, R. D. *Inorg. Chem.* **1972**, *11*, 2192.
(24) Gillespie, R. J.; Spekkens, P. H. *Isr. J. Chem.* **1978**, *17*, 11.
(25) Christe, K. O.; Schack, C. J. *Adv. Inorg. Chem. Radiochem.* **1976**, *18*, 319.
(26) Christe, K. O.; Dixon, D. A. Presented at the 16th Winter Fluorine Conference, St. Petersburg, FL, Jan 12−17, 2003.
(27) Christe, K. O.; Jenkins, H. D. B. *J. Am. Chem. Soc.* **2003**, *125*, 9457.
(28) Gillespie, R. J.; Hargittai, I. In *The VSEPR Model of Molecular Geometry*; Allyn and Bacon: Boston, 1991.
(29) Nakamoto, K. *Infrared and Raman Spectra of Inorganic and Coordination Compounds, Part A*, 5th ed.; Wiley & Sons: New York, 1997; pp 209−211.
(30) Claassen, H. H.; Huston, J. L. *J. Chem. Phys.* **1971**, *55*, 1505.
(31) Beattie, I. R.; Blayden, H. E.; Crocombe, R. A.; Jones, P. J.; Ogden, J. S. *J. Raman Spectrosc.* **1976**, *4*, 313.
(32) Hope, E. G.; Levason, W.; Ogden, J. S. *J. Chem. Soc., Dalton Trans.* **1988**, 61.
(33) Bougon, R.; Buu, B.; Seppelt, K. *Chem. Ber.* **1993**, *126*, 1331.
(34) Gerken, M.; Schrobilgen, G. J. *Coord. Chem. Rev.* **2000**, *197*, 335.
(35) Gillespie, R. J. In *Noble-Gas Compounds*; Hyman, H. H., Ed.; University of Chicago Press: Chicago, 1963; pp 333−339.
(36) Dibeler, V. H.; Liston, S. K. *J. Chem. Phys.* **1968**, *48*, 4765.
(37) Christe, K. O.; Wilson, W. W. *J. Fluorine Chem.* **1990**, *47*, 117.
(38) Christe, K. O.; Wilson, W. W.; Wilson, R. D.; Bau, R.; Feng, J. *J. Am. Chem. Soc.* **1990**, *112*, 7619.
(39) Emara, A. A. A.; Schrobilgen, G. J. *Inorg. Chem.* **1992**, *31*, 1323.
(40) Schrobilgen, G. J. *J. Chem. Soc., Chem. Commun.* **1988**, 863.

Table 1. Summary of Crystal Data and Refinement Results for $[NO]_2[BrO_3F_2][F]$ and $[N(CH_3)_4][BrO_3F_2]$

	$[NO]_2[BrO_3F_2][F]$	$[N(CH_3)_4][BrO_3F_2]$
space group	*C2/c*	*P4/nmm*
a (Å)	9.892(3)	8.5718(7)
b (Å)	12.862(4)	8.5718(7)
c (Å)	10.141(4)	5.8117(6)
β (deg)	105.38(2)	90
V (Å^3)	1246.0(7)	427.02(7)
Z	4	2
mol wt (g mol^{-1})	244.88	240.03
ρ_{calcd} (g cm^{-3})	2.616	1.867
T (°C)	−173	−173
μ (mm^{-1})	6.66	4.81
R_1[a]	0.0671	0.0314
wR_2[b]	0.1813	0.0761

[a] $R_1 = \sum||F_o| - |F_c||/\sum(|F_o|)$ for $I > 2\sigma(I)$. [b] $wR_2 = \sum|(|F_o| - |F_c|)w^{1/2}|/\sum(|F_o|w)$ for $I > 2\sigma(I)$.

mixture of $[N(CH_3)_4][BrO_3F_2]$ and $[N(CH_3)_4)][F]$, providing no evidence for $[N(CH_3)_4]_2[BrO_3F_3]$ formation.

The synthesis of $[N(CH_3)_4][ClO_3F_2]$ was attempted by the reaction of $[N(CH_3)_4][F]$ at −40 °C with neat ClO_3F and with ClO_3F dissolved in CH_3CN solvent. Raman spectroscopy failed to provide evidence for $[N(CH_3)_4][ClO_3F_2]$ formation, which is consistent with earlier attempts to synthesize salts of the $ClO_3F_2^-$ anion by reaction of ClO_3F with the weaker fluoride ion donors CsF[25] and NO_2F.[25]

X-ray Crystal Structures of $[NO]_2[BrO_3F_2][F]$ and $[N(CH_3)_4][BrO_3F_2]$. Unit cell parameters and refinement statistics for $[NO]_2[BrO_3F_2][F]$ and $[N(CH_3)_4][BrO_3F_2]$ at −173 °C are given in Table 1, and geometric parameters are given in Table 2.

(a) $[NO]_2[BrO_3F_2][F]$. The X-ray crystal structure of $[NO]_2[BrO_3F_2][F]$ (Figure 1) is fully ordered, providing accurate geometric parameters for the $BrO_3F_2^-$ anion. The asymmetric unit of this salt is best described in terms of two crystallographically unique $BrO_3F_2^-$ and NO^+ ions and a single F^- anion, with each NO^+ and F^- ion having a symmetry-related position.

The $BrO_3F_2^-$ anion geometry is based upon a trigonal bipyramidal VSEPR arrangement in which the larger steric demands of the double bond pair domains of the oxygen ligands require that they occupy the equatorial positions. The minor distortions of the O−Br−O (118.2(2)−123.5(5)°) and O−Br−F (89.4(3)−90.7(2)°) bond angles from their ideal 120 and 90° values are attributed to solid-state packing effects. The position of the Br−O(3) bond on the 2-fold axis results in each anion having two unique Br−O bonds and two equivalent Br−F bonds. As a result, there are four unique Br−O bond lengths that are the same within $\pm 3\sigma$, with a range of 1.593(7)−1.610(5) Å and an average value of 1.601(7) Å.

The Br−F bond lengths differ significantly for the two crystallographically independent anions at $\pm 3\sigma$ (Br(1)−F(1), 1.872(4) Å; Br(2)−F(2), 1.849(5) Å) and are attributable to different Br−F···N and Br−F···O contacts between the NO^+ cations and the fluorine ligands of the $BrO_3F_2^-$ anions (Figure 1c,d). Each fluorine atom of the crystallographically independent $BrO_3F_2^-$ anions has four contacts with three NO^+ cations such that the Br−F···$[NO]_3$ coordination is a distorted tetrahedral arrangement with different contacts to F(1) and F(2). Two cation contacts to F(1) are of the N−O···F type, with F···O distances of 2.746 and 2.854 Å, and N−O···F angles of 132.1 and 143.8°, respectively. The remaining contacts to F(1) involve both atoms of the same NO^+ cation with N···F and O···F distances of 2.631 and 2.852 Å, respectively, and an O−N···F angle of 90.8°. Two contacts to F(2) involve both atoms of the same NO^+ cation, with N···F and O···F distances of 2.544 and 3.000 Å, respectively, and an O−N···F angle of 105.9°. The two remaining contacts to F(2) are of the N−O···F (2.847 Å) and O−N···F (2.827 Å) types with N−O···F and O−N···F angles of 136.3 and 116.3°, respectively. The O···F contacts to both crystallographically independent anions are close to the sum of the fluorine and oxygen van der Waals radii (2.75,[41] 2.99 Å[42]) and are expected to be long as a result of the negative charges on the oxygen and fluorine atoms. In contrast, the N···F contacts are shorter than the sum of the fluorine and nitrogen van der Waals radii (2.85,[41] 3.08 Å[42]). Although there are two N···F contacts to F(2), with the shorter of these (2.544 Å) being nearly 0.10 Å less than the single N···F(1) (2.631 Å) contact, the Br−F(1) bond is significantly longer than the Br−F(2) bond. The difference may arise from the π-acceptor properties of NO^+ that result from its $\sigma_g^2\sigma_u^{*2}\sigma_g^2\pi_u^4\pi_g^{*0}$ electronic configuration. Transfer of electron density from the anion to the cation is expected when the LUMO (π_g^{*0}) molecular orbital is directed toward the electron donor atom. The ideal π-acceptor orientation for NO^+ only occurs for F(1) (O(6B)−N(2A)···F(1), 90.8°) and

Table 2. Bond Lengths and Bond Angles for $[NO]_2[BrO_3F_2][F]$ and $[N(CH_3)_4][BrO_3F_2]$

$[NO]_2[BrO_3F_2][F]$

bond lengths (Å)		bond angles (deg)	
Br(1)−O(1)	1.599(7)	O(1)−Br(1)−O(2)	119.7(2)
Br(1)−O(2)	1.602(5)	O(1)−Br(1)−F(1)	90.4(1)
Br(1)−F(1)	1.872(4)	F(1)−Br(1)−F(1A)	179.3(3)
Br(2)−O(3)	1.593(7)	O(2)−Br(1)−F(1)	89.9(3)
Br(2)−O(4)	1.610(6)	O(3)−Br(2)−O(4)	118.2(3)
Br(2)−F(2)	1.849(5)	O(3)−Br(2)−F(2)	90.8(2)
N(1)−O(5)	1.038(9)	O(4)−Br(2)−F(2)	89.8(3)
N(2)−O(6)	1.066(8)	F(2)−Br(2)−F(2A)	178.5(3)
O(5A)···F(1)	2.746	N(1A)−O(5A)···F(1)	132.1
O(6A)···F(1)	2.854	N(2B)−O(6A)···F(1)	143.8
O(6B)···F(1)	2.852	O(6B)−N(2A)···F(1)	90.8
N(2A)···F(1)	2.631	N(1B)−O(5B)···F(2)	136.3
O(5B)···F(2)	2.847	O(6A)−N(2A)···F(2)	116.3
O(5A)···F(2)	3.000	O(5A)−N(1A)···F(2)	105.9
N(1A)···F(2)	2.544	O(5)−N(1)···F(3)	105.5
N(2B)···F(2)	2.827	O(5A)−N(1A)···F(3)	114.4
N(1)···F(3)	2.032	O(6)−N(2)···F(3)	103.4
N(2)···F(3)	2.216	O(6A)−N(2A)···F(3)	102.3
N(1A)···F(3)	2.412		
N(2A)···F(3)	2.214		
O(6)···F(3)	2.672		
O(6A)···F(3)	2.654		
O(5)···F(3)	2.517		
O(5A)···F(3)	2.954		

$[N(CH_3)_4][BrO_3F_2]$

bond lengths (Å)		bond angles (deg)	
Br−O(1)	1.600(3)	O(1)−Br−O(2)	118.7(5)
Br−O(2)	1.44(1)	O(1)−Br−F(1)	98.5(3)
Br−F(1)	1.77(6)	O(2)−Br−F(1)	85.9(4)
N−C	1.496(2)	C−N−C(A)	109.2(1)
C−H(1)	0.924	C−N−C(B)	110.0(2)
C−H(2)	0.908		
BrO(1)···Br(B)	4.21		

(41) Pauling, L. *The Nature of the Chemical Bond and the Structure of Molecules and Crystals*, 3rd ed.; Cornell University Press: Ithaca, NY, 1960; p 260.
(42) Bondi, A. *J. Phys. Chem.* **1964**, *68*, 441.

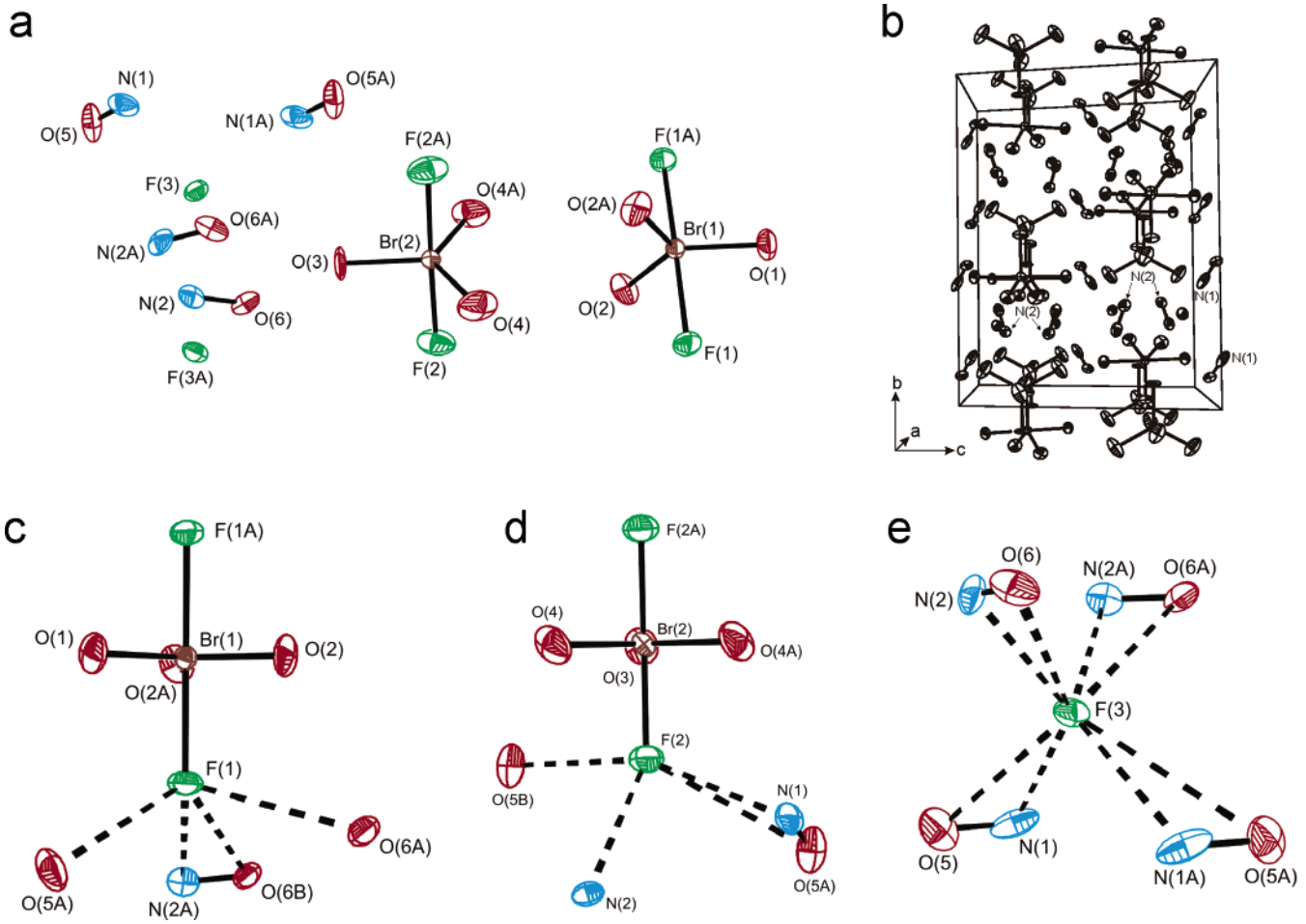

Figure 1. (a) Structural unit and (b) packing diagram of $[NO]_2[BrO_3F_2][F]$. The coordination environments of F(1), F(2), and F(3) are shown in (c), (d), and (e), respectively. Thermal ellipsoids are shown at the 50% probability level.

results in elongation of the Br−F(1) bond. The N(1)−O(5) (1.038(9) Å) and N(2)−O(6) (1.066(8) Å) bond lengths are equivalent to within $\pm 3\sigma$ and therefore cannot be used to correlate the O−N···F interactions with Br−F(1) bond elongation. The existence of two discreet NO^+ cations and their bond length differences are, however, confirmed by the observation of two N−O stretching frequencies in the Raman spectrum of the salt (see Vibrational Spectra of $[M][BrO_3F_2]$).

The fluoride ion (F(3)) of $[NO]_2[BrO_3F_2][F]$ is tetrahedrally coordinated to four NO^+ cations by means of long N···F contacts (2.216−2.412 Å; Figure 1e), which are significantly longer than the N−F bond length of NOF (1.52 Å),[43,44] but shorter than the N···F contacts to the $BrO_3F_2^-$ anions (2.544−2.631 Å), reflecting the stronger Lewis basicity of the fluoride ion. Although none of the O−N···F contacts display the ideal 90° angle that maximizes the π-acceptor interaction with the cation, the cations are coordinated side-on to the fluoride ion with O−N···F angles (102.3−111.4°) and O···F(3) contact distances (2.517−2.945 Å) that lie within or close to the sum of the van der Waals radii for oxygen and fluorine (vide supra). Coordination of the NO^+ cations to the fluoride ion presumably serves to stabilize the $[NO]_2[BrO_3F_2][F]$ salt by reducing the cation interactions with the fluorine ligands of the $BrO_3F_2^-$ anions. This may account for failure to form $[NO][BrO_3F_2]$ which, in the absence of fluoride ions in the crystal lattice, is expected to result in stronger $ON^+\cdots F-BrO_3F$ contacts and destabilization of the salt with respect to $[NO]_2[BrO_3F_2][F]$ and BrO_3F formation (eq 3).

$$2[NO][BrO_3F_2] \rightarrow [NO]_2[BrO_3F_2][F] + BrO_3F \qquad (3)$$

(b) $[N(CH_3)_4][BrO_3F_2]$. The crystal structure of $[N(CH_3)_4][BrO_3F_2]$ (Figure S1) is consistent with an ionic formulation, exhibiting well-separated and weakly interacting cations and anions. While the $N(CH_3)_4^+$ cations are fully ordered, the $BrO_3F_2^-$ anions display a 2-fold (i.e., 90°) disorder along the Br−O(1) axis, giving rise to two equally populated anion orientations (Figure S1a). The disorder reflects the solid-state packing arrangement of the salt, which can be described as staggered columns of cations and anions running parallel to the *c*-axis (Figure S1b). Whereas the disorder does not allow the extraction of meaningful bond lengths and bond angles involving disordered oxygen and fluorine atoms, the Br−O(1) bond length (1.600(3) Å) is reliable and is in excellent agreement with the Br−O distances determined for $[NO]_2[BrO_3F_2][F]$ (vide supra). Although two possible positions for the disordered oxygen and fluorine atoms can be resolved, the Br−O(2) (1.44(1) Å) and Br−F(1) (1.77(6) Å) bond lengths are both artificially contracted. The O(1)−Br−O(2) and O(1)−Br−F(1) bond angles, which should be 120 and 90°, are 118.7(5) and 98.5(3)°, respectively, and are less affected by the disorder.

(43) Magnuson, D. W. *J. Chem. Phys.* **1951**, *19*, 1071.
(44) Stephenson, C. V.; Jones, E. A. *J. Chem. Phys.* **1952**, *20*, 135.

(c) Bond Length Comparisons among Known Br(VII) Species. The nondisordered Br−O bond lengths obtained from the crystal structures of $[N(CH_3)_4][BrO_3F_2]$ and $[NO]_2[BrO_3F_2][F]$ are very similar to the average bond length of BrO_4^- (1.603(16) Å)[45−47] despite the higher coordination number of $BrO_3F_2^-$. As anticipated, the Br−O and Br−F bonds are longer and more polar than the Br−F (1.708(3)) and Br−O (1.582(1) Å) bond of neutral BrO_3F[48] and have bond orders that are less than those of BrO_3F (see Computational Results).

Although the average bond lengths for AsF_6^- (1.70(2) Å),[49] SeF_6 (1.69(1) Å),[50] and BrF_6^+ (1.666(11) Å)[51] do not show a significant contraction with increasing positive charge, the F···F bond orders[51] and ligand packings of the XF_6^+ (X = Cl, Br, I) cations[51,52] indicate that the fluorine ligands of BrF_6^+ are not close-packed. Ligand−ligand repulsions also do not appear to strongly influence the bond lengths of lower-coordinate Br(VII) species (vide supra). Thus, the anticipated trend of decreasing Br−F bond length with increasing net positive charge is observed for $BrO_3F_2^-$ (1.861(16) Å), BrO_3F (1.708(3) Å),[48] and BrF_6^+ (1.666(11) Å).[51]

Vibrational Spectra of $[M][BrO_3F_2]$ (M = K, Rb, Cs, $N(CH_3)_4$) and $[NO]_2[BrO_3F_2][F]$. Of the 12 fundamental modes of vibration ($\Gamma_{vib} = 2A_1' + 2A_2'' + 3E' + E''$) predicted for $BrO_3F_2^-$ (Figure S2), the $\nu_1(A_1')$, $\nu_2(A_1')$, $\nu_5(E')$, $\nu_6(E')$, $\nu_7(E')$, and $\nu_8(E'')$ modes are ideally only Raman-active and the $\nu_3(A_2'')$, $\nu_4(A_2'')$, $\nu_5(E')$, and $\nu_6(E')$ modes are ideally only infrared-active.

The Raman spectra (−163 °C) of α-$[Cs][BrO_3F_2]$, β-$[Cs][BrO_3F_2]$, $[Rb][BrO_3F_2]$, $[K][BrO_3F_2]$, $[N(CH_3)_4][BrO_3F_2]$, and $[NO]_2[BrO_3F_2][F]$ and the room-temperature infrared spectrum of β-$[Cs][BrO_3F_2]$ are shown in Figure 2. The vibrational assignments for the $BrO_3F_2^-$ anion (Table 3) were made with the assistance of quantum mechanical calculations in Tables 3 and S1 (also see Computational Results and Supporting Information) and by comparison with the vibrational spectra of XeO_3F_2[30] and OsO_3F_2.[31,32] Trends in the BrO_3 and BrF_2 stretching frequencies reflect the anticipated cation−anion interactions in the salt, paralleling the cation charge-to-radius ratios,[27] which increase in the order $N(CH_3)_4^+ < Cs^+ < Rb^+ < K^+$ (see Supporting Information).

(a) $[M][BrO_3F_2]$ (M = Cs, Rb, K). The low-temperature α-phase of $[Cs][BrO_3F_2]$ exhibits six Raman-active bands, consistent with D_{3h} symmetry. The most intense band in the spectrum (802 cm^{-1}) was assigned to the symmetric BrO_3 stretch, $\nu_1(A_1')$, and the band at 896 cm^{-1} to the asymmetric BrO_3 stretch, $\nu_5(E')$. These assignments are supported by the calculated frequencies and the anticipated trend, $\nu_s < \nu_{as}$, although it is noteworthy that the order of the $\nu_1(A_1')$ and $\nu_5(E')$ frequencies is reversed for OsO_3F_2[31,32] (see Symmetry Force Constants Derived from B-Matrix Analyses). The bands at 229, 383, 414, and 433 cm^{-1} were assigned to $\nu_7(E')$, $\nu_6(E')$, $\nu_8(E'')$, and $\nu_2(A_1')$, respectively, by analogy with XeO_3F_2[30] and monomeric OsO_3F_2.[31]

The high-temperature phase, β-$[Cs][BrO_3F_2]$, is easily distinguished from the α-phase on the basis of frequency shifts, splittings of the Raman-active modes, and additional weak bands in the Raman spectrum, which are assigned to the formally Raman-inactive $\nu_3(A_2'')$ and $\nu_4(A_2'')$ modes. The $\nu_1(A_1')$ (807 cm^{-1}) and $\nu_5(E')$ (903 cm^{-1}) BrO_3 stretches are at somewhat higher frequencies in the β-phase than in the α-phase. The $\nu_5(E')$ band is also significantly broadened with shoulders at 899 and 908 cm^{-1}, which are presumed to arise from site-symmetry lowering and vibrational coupling within the unit cell. The splittings of the $\nu_6(E')$ (386, 392 cm^{-1}) and $\nu_8(E'')$ (404, 409 cm^{-1}) modes are also consistent with the latter assumption. The reduced symmetry, inferred from the splitting of the degenerate BrO_3 stretches and bends, also allows the observation of the $\nu_3(A_2'')$ and $\nu_4(A_2'')$ modes. The BrO_3 out-of-plane bend ($\nu_3(A_2'')$) was assigned at 449 cm^{-1}, while the higher frequency bands (485, 497 cm^{-1}) were assigned to the antisymmetric BrF_2 stretch ($\nu_4(A_2'')$). The latter modes were observed at 468 and 504 cm^{-1} in the infrared spectrum of β-$[Cs][BrO_3F_2]$ along with the $\nu_1(A_1')$ (800 cm^{-1}) and $\nu_5(E')$ (881, 900, 909 cm^{-1}) modes (Figure 2b).

The spectra of $[K][BrO_3F_2]$ and $[Rb][BrO_3F_2]$ were similar to that of β-$[Cs][BrO_3F_2]$ and were assigned accordingly. In contrast with $[Cs][BrO_3F_2]$, only single phases were observed for $[K][BrO_3F_2]$ and $[Rb][BrO_3F_2]$, which may reflect the higher temperatures required for their syntheses. The symmetric and antisymmetric BrO_3 stretching frequencies of the K^+ and Rb^+ salts are slightly higher in frequency than in β-$[Cs][BrO_3F_2]$ and exhibit larger splittings of the $\nu_5(E')$ mode, and the splittings of the $\nu_2(A_1')$, $\nu_6(E')$, and $\nu_8(E'')$ modes are somewhat more complex in the K^+ and Rb^+ salts than in β-$[Cs][BrO_3F_2]$. Although the splittings of the degenerate E′ modes are attributable to site-symmetry lowering of the anion in the solid state, the splittings of the nondegenerate $\nu_2(A_1')$ mode in the K^+ (420, 425 cm^{-1}) and Rb^+ (417, 427 cm^{-1}) salts indicate that vibrational coupling within their respective unit cells must also occur. The formally Raman-inactive A_2'' modes appear as weak bands in the Raman spectra of $[K][BrO_3F_2]$ and $[Rb][BrO_3F_2]$. The asymmetric BrF_2 stretching mode, $\nu_4(A_2'')$, is factor-group split and has similar band contours in the spectra of $[K][BrO_3F_2]$ (506, 523 cm^{-1}), $[Rb][BrO_3F_2]$ (497, 512 cm^{-1}), and β-$[Cs][BrO_3F_2]$ (485, 497 cm^{-1}). The BrO_3 bend, $\nu_3(A_2'')$, which is a single band in $[K][BrO_3F_2]$ (457 cm^{-1}) and $[Rb][BrO_3F_2]$ (455 cm^{-1}) but is split in β-$[Cs][BrO_3F_2]$ (433, 449), is less sensitive to the nature of the counterion.

(b) $[N(CH_3)_4][BrO_3F_2]$. The Raman spectrum of $[N(CH_3)_4][BrO_3F_2]$ is characteristic for a $BrO_3F_2^-$ anion and a $N(CH_3)_4^+$ cation.[38,53−55] The $BrO_3F_2^-$ anion disorder (see X-ray Crystal Structures of $[NO]_2[BrO_3F_2][F]$ and $[N(CH_3)_4][BrO_3F_2]$) prevents an unambiguous correlation between the free ion (D_{3h}), site (C_{4v}), and crystallographic unit cell (D_{4h}) symmetries; however, the observed broadening or splitting of the $\nu_2(A_1')$, $\nu_5(E')$, $\nu_6(E')$, $\nu_7(E')$, and $\nu_8(E'')$ modes is indicative of factor-group splitting. The BrO_3 stretches occur at 801 cm^{-1} ($\nu_1(A_1')$) and 896 cm^{-1} ($\nu_5(E')$), with the former again being the most

(45) Siegel, S.; Tani, B.; Appelman, E. *Inorg. Chem.* **1969**, *8*, 1190.
(46) Gebert, E.; Peterson, S. W.; Reis, A. H.; Appelman, E. H. *J. Inorg. Nucl. Chem.* **1981**, *43*, 3085.
(47) Gallucci, J. C.; Gerkin, R. E.; Reppart, W. J. *Acta Crystallogr.* **1989**, *C45*, 701.
(48) Appelman, E. H.; Beagley, B.; Cruickshank, D. W. J.; Foord, A.; Rustad, S.; Ulbrecht, V. *J. Mol. Struct.* **1976**, *35*, 139.
(49) Lehmann, J. F.; Dixon, D. A.; Schrobilgen, G. J. *Inorg. Chem.* **2001**, *40*, 3002.
(50) Ewing, V. C.; Sutton, L. E. *Trans. Faraday Soc.* **1963**, *59*, 1241.
(51) Lehmann, J. F.; Schrobilgen, G. J.; Christe, K. O.; Kornath, A.; Suontamo, R. J. *Inorg. Chem.* **2004**, *43*, 6905.
(52) Robinson, E. A.; Gillespie, R. J. *Inorg. Chem.* **2003**, *42*, 3865.
(53) Berg, R. W. *Spectrochim. Acta* **1978**, *34A*, 655.
(54) Kabisch, G.; Klose, M. *J. Raman Spectrosc.* **1978**, *7*, 311.
(55) Mercier, H. P. A.; Sanders, J. C. P.; Schrobilgen, G. J. *J. Am. Chem. Soc.* **1994**, *116*, 2921.

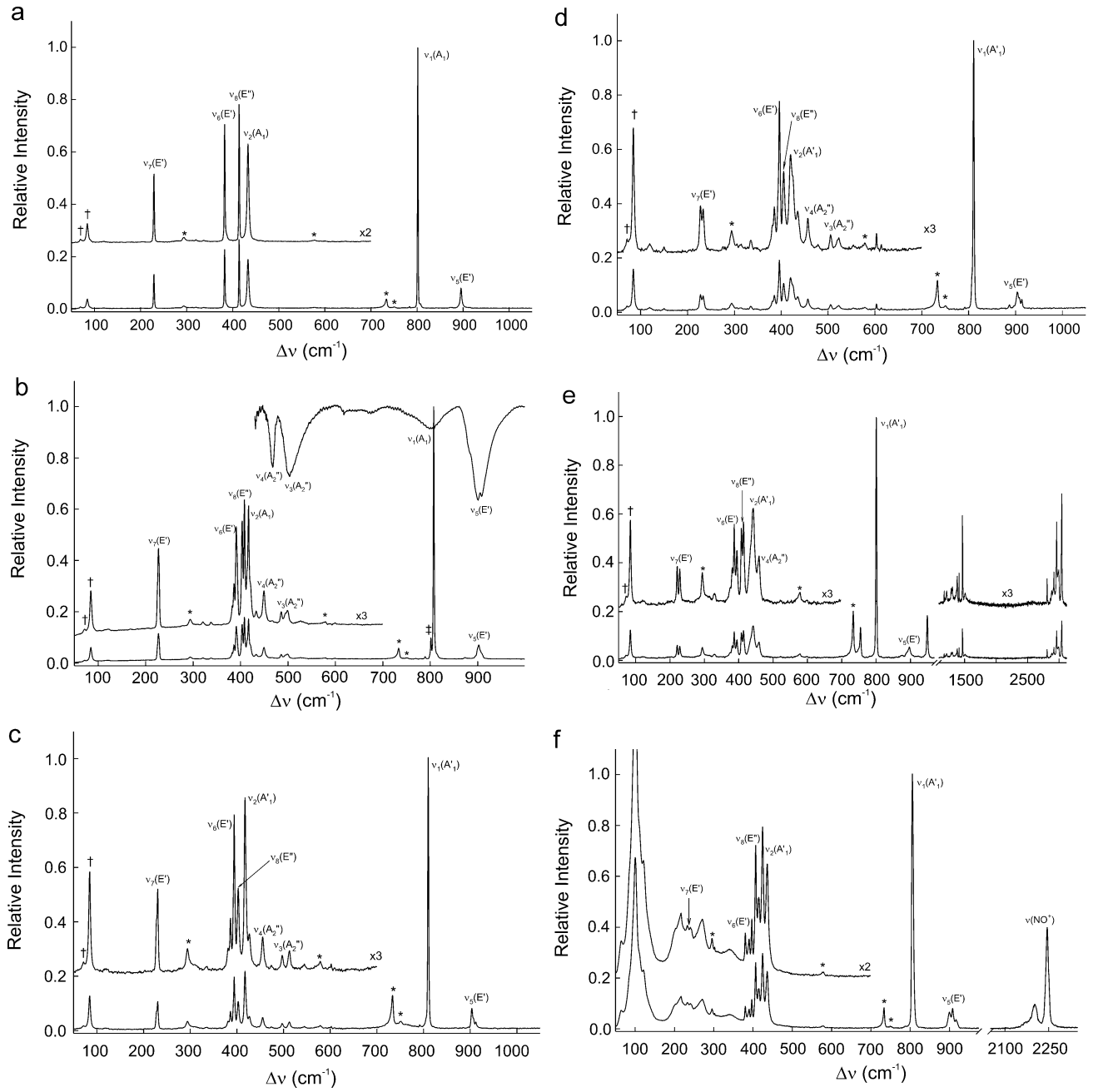

Figure 2. Raman spectra (recorded at −163 °C) of (a) α-$[Cs][BrO_3F_2]$; (b) β-$[Cs][BrO_3F_2]$, the band at 802 cm^{-1} (‡) arises from residual α-$[Cs][BrO_3F_2]$ and the upper trace is the room-temperature infrared spectrum of β-$[Cs][BrO_3F_2]$ in an AgCl pellet; (c) $[Rb][BrO_3F_2]$; (d) $[K][BrO_3F_2]$; (e) $[N(CH_3)_4][BrO_3F_2]$, unlabeled bands arise from the $N(CH_3)_4^+$ cation and the band at 460 cm^{-1}, tentatively assigned to $\nu_4(A_2'')$ of $BrO_3F_2^-$, may alternatively be assigned to, or overlap with, $\nu_{19}(F_2)$ of $N(CH_3)_4^+$; (f) $[NO]_2[BrO_3F_2][F]$. Asterisks (*) denote FEP sample tube lines, and daggers (†) denote instrumental artifacts.

intense feature in the spectrum and the latter exhibiting some broadening. The frequencies of the remaining modes and their relative intensities are also in good agreement with those of the alkali metal salts. The formally Raman-inactive $\nu_3(A_2'')$ was not observed, and the band at 460 cm^{-1} is tentatively assigned to the formally Raman-inactive $\nu_4(A_2'')$ mode of $BrO_3F_2^-$, which may overlap with $\nu_{19}(F_2)$ of the $N(CH_3)_4^+$ cation.[38,53−55]

(c) $[NO]_2[BrO_3F_2][F]$. The Raman spectrum of $[NO]_2[BrO_3F_2][F]$ is similar to that of the alkali metal and $N(CH_3)_4^+$ salts, with the added exception that the low-frequency region (100−340 cm^{-1}) is dominated by broad bands of medium intensity. It is likely that a number of these bands arise from O−N···F(1,2,3) bending and ON···F(1,2,3) stretching modes, which are expected to be significantly lower in frequency than those of ONF (492 and 735 cm^{-1}, respectively)[56] as a result of the long N···F contact distances and are broadened because there are several such contacts (Figure 1 and Table 2). The presence of two bands in the N−O stretching region (2203, 2246 cm^{-1}) is in accord with the two crystallographically unique cation sites (Figure 1c,d). Although the N−O stretching frequencies agree more closely with that of NO^+ (2273 cm^{-1})[57] than with that of gaseous ONF (1844 cm^{-1}),[58−60] the low-frequency shift is

(56) Smardzewski, R. R.; Fox, W. B. *J. Am. Chem. Soc.* **1974**, *96*, 304.
(57) Babaeva, V. P.; Rosolovskii, V. Y. *Russ. J. Inorg. Chem.* **1971**, *16*, 471.
(58) Jones, E. A.; Woltz, P. J. H. *J. Chem. Phys.* **1950**, *18*, 1516.
(59) Magnuson, D. W. *J. Chem. Phys.* **1952**, *20*, 380.
(60) Jones, L. H.; Asprey, L. B.; Ryan, R. R. *J. Chem. Phys.* **1967**, *47*, 3371.

Table 3. Vibrational Frequencies, Intensities, and Assignments for the $XO_3F_2^-$ (X = Cl, Br) Anions

		$BrO_3F_2^-$ [a]								$ClO_3F_2^-$
			Raman				IR	Raman		
assignment (D_{3h})[c]		calcd[b]	K^+	Rb^+	α-Cs^+	β-Cs^+	β-Cs^+[d]	$[NO^+]_2[F^-]$[e]	$N(CH_3)_4^+$ [f]	calcd[b]
$\nu_1(A_1')$	$\nu_s(XO_3)$	788(100)[0]	811(100)	810(100)	802(100)	807(100)	800[w,br]	806(100)	801(100)	875(100)[0]
$\nu_2(A_1')$	$\nu_s(XF_2)$	435(45)[0]	435(6)	427(5)	433(19)	421(sh)		436(21)	442(14)	364(40)[0]
			420(13)	417(22)		417(17)		425(28)	434(sh)	
$\nu_3(A_2'')$	$\nu_{as}(XF_2)$	529(0)[389]	523(2)	512(3)		497(3)	504[m]			630(0)[376]
			506(3)	497(3)		485(3)				
$\nu_4(A_2'')$	$\delta(XO_3)$	447(0)[17]	457(5)	455(5)		449(6)	468[m]		460(6)[g]	459(0)[317]
	oop					433(3)				
$\nu_5(E')$	$\nu_{as}(XO_3)$	883(32)[304]	914(5)	912(3)	896(8)	908(sh)	909[s]	917(3)	896(5)	1144(24)[614]
			908(5)	907(sh)		903(7)	900[s]	908(7)		
			904(7)	904(8)		899(sh)	881[sh]	900(6)		
$\nu_6(E')$	$\delta(XO_3)$	378(26)[76]	397(19)	394(20)	383(23)	392(14)		397(10)	395(3)	513(29)[54]
	ip		393(sh)	386(7)		386(7)		390(5)	389(4)	
				381(3)		383(sh)		381(7)	382(2)	
$\nu_7(E')$	$\delta(XF_2)$	207(6)[<1]	227(6)	228(sh)	229(13)	227(12)		240(sh)	228(1)	247(5)[4]
			233(6)	231(11)				233(sh)	222(1)	
$\nu_8(E'')$	$\rho_r(XF_2)$	384(24)[0]	406(11)	403(11)	414(27)	409(18)		415(14)	414(12)	456(19)[0]
						404(15)		407(25)	408(11)	

[a] All experimental frequencies are from Raman spectra, except for β-[Cs][BrO_3F_2] for which infrared frequencies are also provided. Frequencies are given in cm^{-1}. All Raman spectra were recorded at −163 °C in FEP sample tubes. The experimental intensities, given in parentheses, are scaled relative to the intensity of the ν_1 mode, which is assigned a value of 100. The abbreviation, sh, denotes a shoulder. [b] MPW1PW91/DZVP. The calculated absolute Raman intensities in amu $Å^{-4}$ may be obtained by dividing the relative calculated intensities by the following scaling coefficients: 2.45 for $BrO_3F_2^-$ and 2.38 for $ClO_3F_2^-$. [c] The symbols ν, δ, and ρ_r denote stretch, bend, and rock, respectively. The abbreviations s, as, oop, and ip denote symmetric, antisymmetric, out-of-plane, and in-plane, respectively. [d] The infrared spectrum of β-[Cs][BrO_3F_2] was obtained in a AgCl pellet at ambient temperature. The abbreviations w, m, s, and br denote weak, medium, strong, and broad infrared lines, respectively. [e] The NO^+ stretches occur at 2203(8) and 2246(31) cm^{-1}. Additional broad bands were observed at 340(6), 302(6), 295(8), 271(11), 255(10), 233(11), 217(13), 205 sh, 121(23), 100(68), 65(7) cm^{-1} and are tentatively assigned to O−N···F(1,2,3) bending and ON···F(1,2,3) stretching modes associated with NO^+ and $BrO_3F_2^-$ interactions in the crystal lattice and to lattice modes. [f] Bands at 3042(16), 2995(6), 2919(5), 2881(3), 2866(2), 2809(5), 1469(11), 1466(13), 1412(5), 1286(3), 1184(2), 1177(3), 949(19), 755(14), 460(6), and 329(2) cm^{-1} were assigned to $N(CH_3)_4^+$ by comparison with previous assignments given in refs 38, 54−56. [g] This band may result from the overlap of the formally Raman-inactive $\nu_4(A_2'')$ mode and $\nu_{19}(F_2)$ of the $N(CH_3)_4^+$ cation.

consistent with significant interactions between the NO^+ cations and the $BrO_3F_2^-$ and F^- anions. The splittings of the $\nu_2(A_1')$, $\nu_5(E')$, $\nu_6(E')$ $\nu_7(E')$, and $\nu_8(E'')$ modes of $BrO_3F_2^-$ in the Raman spectrum of [NO]$_2$[BrO_3F_2][F] are consistent with factor-group splitting (see complementary discussion in Supporting Information and Table S2).

NMR Spectroscopy. The ^{19}F, ^1H, and ^{13}C NMR spectra of [$N(CH_3)_4$][BrO_3F_2] dissolved in CH_3CN at −40 °C were obtained from a sample that had been stored at −196 °C and had not been previously warmed above −40 °C. The ^{19}F NMR spectrum exhibited a single resonance at 237.0 ppm ($\Delta\nu_{1/2}$, 360 Hz), which is assigned to the chemically equivalent fluorines of the $BrO_3F_2^-$ anion. The ^{19}F chemical shift of $BrO_3F_2^-$ is significantly more shielded than that of BrF_6^+ (339,[3] 337[3,61] ppm) and BrO_3F (269−274 ppm),[24] with the general trend of increased deshielding with increasing formal charge being adhered to for these Br(VII) species. The broad line width is attributed to the nearly completely quadrupole-collapsed $^1J(^{79,81}Br-^{19}F)$ spin−spin coupling, as is the case for BrO_3F ($\Delta\nu_{1/2}$, 70−217 Hz).[24] Quadrupolar collapse in these lower symmetry species contrasts with that of the highly symmetric BrF_6^+ cation, for which the near-zero electric field gradient at the octahedrally coordinated quadrupolar ^{79}Br and ^{81}Br ($I = {}^3/_2$) nuclei results in slow quadrupolar relaxation and observation of the $^1J(^{79,81}Br-^{19}F)$ couplings.[3,51] The ^1H and ^{13}C resonances of the $N(CH_3)_4^+$ cation were observed at 3.0[37] and 55.4 ppm, respectively, with a $^1J(^{13}C-^1H) = 143$ Hz.

Computational Results. (a) $BrO_3F_2^-$ and $ClO_3F_2^-$ Geometries. Although the energy-minimized gas-phase structures of BrO_3F, ClO_3F, $BrO_3F_2^-$, and $ClO_3F_2^-$ determined by use of the HF, MP2, and LDF (MPW1PW91) (Table S3) methods are comparable, only the LDF results are referred to in the present discussion. The calculated geometries of the parent oxide fluorides, BrO_3F and ClO_3F, were used as benchmarks for comparison of the effects of fluoride ion coordination on the X−O and X−F (X = Cl, Br) bond lengths. The energy-minimized gas-phase structures of *fac*-$BrO_3F_3^{2-}$ and *mer*-$BrO_3F_3^{2-}$ are also provided in Table S3 and are discussed in the Supporting Information.

The geometry of the $BrO_3F_2^-$ anion in [NO]$_2$[BrO_3F_2][F] (see X-ray Crystal Structures of [NO]$_2$[BrO_3F_2][F] and [$N(CH_3)_4$][BrO_3F_2]) exhibited only small distortions from the ideal trigonal bipyramidal geometry, justifying the calculation of $BrO_3F_2^-$ and $ClO_3F_2^-$ constrained to D_{3h} symmetry. The calculated Br−O bond length (1.639 Å) is moderately longer than the average experimental value (1.603(6) Å); however, the difference between the Br−O bond lengths of $BrO_3F_2^-$ and BrO_3F is comparable when determined by theory (0.03 Å) and by experiment (0.01−0.03 Å). The calculated Br−F bond length (1.905 Å) is also slightly longer than the average obtained from the structure of [NO]$_2$[BrO_3F][F]; however, in this instance the difference between the values calculated for $BrO_3F_2^-$ and BrO_3F (0.10 Å) is less than that observed experimentally (0.15 Å). The difference is attributed to significant ON···F−BrO_3F interactions in the solid state that further elongate the Br−F bonds of the anion.

Although attempts to prepare [$N(CH_3)_4$][ClO_3F_2] were unsuccessful, the anion is predicted to be thermodynamically stable with respect to dissociation to ClO_3F and F^- in the gas phase (vide infra). The weak fluoride ion acceptor properties of ClO_3F are reflected in the Cl−F bond lengths of the anion (1.881 Å),

(61) Schroer, T.; Christe, K. O. *Inorg. Chem.* **2001**, *40*, 2415.

which were calculated to be ca. 0.20 Å longer than that for ClO_3F (1.685 Å), in accord with the smaller difference (ca. 0.10 Å) obtained for the bromine analogues. Additional elongation and destabilization of the Cl−F bonds of $ClO_3F_2^-$ relative to that of ClO_3F would be expected in the solid state, where contacts between the fluorine ligands and countercation are likely and may account, in part, for the inability to prepare salts of this anion. The difference (ca. 0.03 Å) between the calculated Cl−O bond lengths of $ClO_3F_2^-$ (1.465 Å) and ClO_3F (1.438 Å) is similar to that calculated for $BrO_3F_2^-$ and BrO_3F.

(b) Enthalpies of Fluoride Ion Attachment to BrO_3F and ClO_3F. The enthalpies of fluoride ion attachment for BrO_3F, $BrO_3F_2^-$, and ClO_3F have been determined by the G2 method (Table S4), which includes fourth order (MP4) and configuration interaction (QCISD) energy corrections. The method differs from the near-local density functional (NLDF)[26] and MP2/PDZ[62] methods used previously. The accuracy of the G2 method was verified by calculating the enthalpies of fluoride ion attachment for HF, COF_2, SO_2, BF_3, and AlF_3 (Table S4), which have accurately determined experimental values and which have been used as benchmarks in previous computational studies.[26,62]

Both BrO_3F and ClO_3F are predicted to be fluoride ion acceptors in the gas phase; however, the enthalpy of fluoride ion attachment is significantly more exothermic for BrO_3F (−261.1 kJ mol^{-1}) than for ClO_3F (−132.3 kJ mol^{-1}). The enthalpy of fluoride ion attachment to BrO_3F, determined in the present study, is 11% less than the value reported earlier (−292 kJ mol^{-1})[26] but is bracketed by the values previously calculated for $XeOF_4$ (−267 kJ mol^{-1}), TeF_6 (−257 kJ mol^{-1}), and XeF_4 (−239 kJ mol^{-1}).[26] In view of the experimentally established stabilities of $XeOF_5^-$,[63] TeF_7^-,[64] and XeF_5^-,[65] it is not surprising that salts of the $BrO_3F_2^-$ anion have proven to be isolable.

The enthalpy of fluoride ion attachment for ClO_3F determined by the G2 method is also lower than that obtained by the NLDF method (−180 kJ mol^{-1}).[26] The present study indicates that the fluoride ion acceptor strength of ClO_3F is intermediate with respect to those of PF_3 (−187.9 kJ mol^{-1}), HF (−154.0 kJ mol^{-1}), NO_2F (−80.3 kJ mol^{-1}), and NOF (−72.8 kJ mol^{-1}) in the gas phase.[62] Although salts of PF_4^-[66,67] and HF_2^-[68] are known, those of $NO_2F_2^-$[69] and NOF_2^- are unknown. The ranking of $ClO_3F_2^-$ within this series is consistent with the minimum enthalpy of fluoride ion attachment (−126 to −146 kJ mol^{-1})[26] generally required for the formation of a stable salt, and inability to prepare $[N(CH_3)_4][ClO_3F_2]$. The fluoride ion acceptor properties of $BrO_3F_2^-$ were also investigated by the G2 method. The positive enthalpies of formation arrived at for the gas-phase formation of *fac*-$BrO_3F_3^{2-}$ (362.1 kJ mol^{-1}) and *mer*-$BrO_3F_3^{2-}$ (367.8 kJ mol^{-1}) indicate that both isomers are unstable and is consistent with the present failed attempts to synthesize $[N(CH_3)_4]_2[BrO_3F_3]$ (see Attempted Syntheses of $[N(CH_3)_4]_2[BrO_3F_3]$ and $[N(CH_3)_4][ClO_3F_2]$ in the Experimental Section).

(c) Vibrational Frequencies of $BrO_3F_2^-$ and $ClO_3F_2^-$. The vibrational frequencies and intensities of $BrO_3F_2^-$ and $ClO_3F_2^-$ were calculated by use of HF, MP2, and LDF (MPW1PW91) (Table S1) methods and were used to assist in the assignment of the experimental vibrational spectra of the $BrO_3F_2^-$ salts. The LDF method provided the most reliable vibrational frequencies and intensities for the $ClO_3F_2^-$ and $BrO_3F_2^-$ anions, which are referred to in the present discussion and in Table 3.

(d) Force Constants for $BrO_3F_2^-$, $ClO_3F_2^-$, XeO_3F_2, and OsO_3F_2. Internal force constants have been previously determined for XeO_3F_2[30,70−72] and OsO_3F_2[71−73] by use of the Wilson FG-matrix method[74] and are now calculated for the $BrO_3F_2^-$ anion by the same method. To complement these studies and to allow for comparisons with the unknown $ClO_3F_2^-$ anion, the symmetry force constants of $BrO_3F_2^-$, $ClO_3F_2^-$, XeO_3F_2, and OsO_3F_2 have been calculated by the B-matrix method,[75] which provides a fully determined force field that includes off-diagonal components.

(i) Internal Force Constants Derived from General Valence Force Field (GVFF) Analyses. The internal force constants and potential energy distributions of $BrO_3F_2^-$, XeO_3F_2, and OsO_3F_2, determined by the FG-matrix method, are summarized in Tables 4 and S5, respectively. The lower f_D value of $BrO_3F_2^-$ with respect to that of XeO_3F_2 is attributed to the higher formal oxidation state of xenon and resulting lower polarities of the Xe−O bonds. Despite the neutral charges and formal +8 oxidation states of osmium and xenon, f_D is significantly greater for OsO_3F_2 than for XeO_3F_2. The difference likely reflects the relative degrees of $d\pi-p\pi$ bonding between the central atom and the oxygen ligands, which is expected to be significant for d^0 species, but a minor contributor in the bonding of the main-group species.[76] The greater Os−O bond strength of OsO_3F_2 is also indicated by the calculated Os−O bond length (1.717 Å), which is ca. 0.08 Å shorter than the calculated Xe−O bond length of XeO_3F_2 (1.802 Å) even though xenon is in row five and osmium is in row six of the periodic table.

The Xe−F and Os−F stretching force constants (f_d) obtained for XeO_3F_2 and OsO_3F_2 in the present work are in good agreement with the previously reported values determined by the FG-matrix method for XeO_3F_2[71,72] and OsO_3F_2,[71] but are somewhat greater than those reported in refs 72 and 73 for OsO_3F_2. The trends among the f_d values for $BrO_3F_2^-$, XeO_3F_2, and OsO_3F_2 are similar to those of f_D and are also attributable to net charge, formal oxidation state of the central atom, and relative degrees of $d\pi-p\pi$ bonding. The smaller difference between the f_d values of XeO_3F_2 and OsO_3F_2 (0.83 mdyne Å^{-1}) when compared with that of their f_D values (1.37 mdyne Å^{-1}) is consistent with the reluctance of fluorine to form multiple bonds.

(62) Christe, K. O.; Dixon, D. A.; McLemore, D.; Wilson, W. W.; Sheehy, J. A.; Boatz, J. A. *J. Fluorine Chem.* **2000**, *101*, 151.
(63) Christe, K. O.; Dixon, D. A.; Sanders, J. C. P.; Schrobilgen, G. J.; Tsai, S. S.; Wilson, W. W. *Inorg. Chem.* **1995**, *34*, 1868.
(64) Selig, H.; Sarig, S.; Abramowitz, S. *Inorg. Chem.* **1974**, *13*, 1508.
(65) Christe, K. O.; Curtis, E. C.; Dixon, D. A.; Mercier, H. P. A.; Sanders, J. C. P.; Schrobilgen, G. J. *J. Am. Chem. Soc.* **1991**, *113*, 3351.
(66) Wermer, P.; Ault, B. S. *Inorg. Chem.* **1981**, *20*, 970.
(67) Christe, K. O.; Dixon, D. A.; Mercier, H. P. A.; Sanders, J. C. P.; Schrobilgen, G. J.; Wilson, W. W. *J. Am. Chem. Soc.* **1994**, *116*, 2850.
(68) Gilbert, A. S.; Sheppard, N. *Spectrochim. Acta, Part A* **1976**, *32*, 923.
(69) Lawlor, L.; Passmore, J. *Inorg. Chem.* **1979**, *18*, 2923.
(70) Natarajan, A.; Chockalingam, K. *Pramana* **1977**, *9*, 573.
(71) Gnanasekaran, S.; Ranganayaki, S.; Gnanasekaran, P.; Sampath Krishnan, S. *Asian J. Chem.* **1989**, *1*, 173.
(72) Mohan, S.; Vasuki, G. *Proc. Natl. Acad. Sci., India, Sect. A* **1989**, *59*, 163.
(73) So, S. P. *Z. Phys. Chem., Neue Folge* **1978**, *109*, 157.
(74) Wilson, E. B. *J. Chem. Phys.* **1941**, *9*, 76.
(75) Komornicki, A.; *BMATRIX*, version 2.0; Polyatomics Research Institute: Palo Alto, CA, 1996.
(76) Reed, A. E.; Schleyer, P. v. R. *J. Am. Chem. Soc.* **1990**, *112*, 1434.

Table 4. Internal and Symmetry Force Constants for $BrO_3F_2^-$, XeO_3F_2, OsO_3F_2, and $ClO_3F_2^-$ and Potential Energy Distributions (PED) Derived from B-Matrix Analyses

internal force constants (GVFF)[a,b]				symmetry force constants (B-matrix)[b,c]				
	$BrO_3F_2^-$	XeO_3F_2	OsO_3F_2		$ClO_3F_2^-$	$BrO_3F_2^-$	XeO_3F_2	OsO_3F_2
f_D	5.86	6.27	7.64	A_1' species:				
f_d	2.15	3.29	4.12	$F_{11} = f_D + 2f_{DD}$	6.98	5.83	5.45	8.73
f_β	1.63	1.36	0.94	$F_{22} = f_d + 2f_{dd}$	1.68	2.09	2.92	4.30
f_α	0.59	0.66	0.46	$F_{12} = 6^{1/2}f_{Dd}$	0.43	0.28	−0.09	0.49
f_{DD}	0.11	−0.07	0.19	A_2'' species:				
f_{dd}	0.28	0.38	0.49	$F_{33} = f_d - f_{dd}$	1.73	2.19	3.04	4.13
f_{Dd}	0.003	−0.0003	0.006	$F_{44} = f_\beta - f_{\beta\beta} - 2f'_{\beta\beta} - 2f''_{\beta\beta}$	2.03	1.65	1.28	0.85
$f_{D\beta}$	0.04	0.005	0.16	$F_{34} = (3(f_{a\beta} - f'_{a\beta}))^{1/2}$	0.78	0.41	0.11	0.61
$f_{D\alpha}$	0.04	0.005	0.06	E′ species:				
$f_{d\beta}$	0.12	−0.13	0.09	$F_{55} = f_D - f_{DD}$	6.97	5.64	5.64	7.63
$f_{\beta\beta}$	0.12	0.20	−0.12	$F_{66} = f_\alpha - f_{\alpha\alpha}$	0.85	0.59	0.43	0.64
$f_{\alpha\alpha}$	−0.08	−0.19	−0.37	$F_{77} = f_\beta + f_{\beta\beta} - f'_{\beta\beta} - f''_{\beta\beta}$	1.57	1.36	1.10	1.18
$f_{\alpha\beta}$	0.11	0.03	0.01	$F_{56} = f'_{D\alpha} - f_{D\alpha}$	−0.08	0.02	0.06	0.14
$f'_{D\beta}$	−0.02	0.01	−0.01	$F_{57} = 2^{1/2}(f_{D\beta} - f'_{D\beta})$	0.24	0.19	0.06	0.15
$f'_{D\alpha}$	−0.02	0.01	−0.03	$F_{67} = -2^{1/2}(f_{\alpha\beta} - f'_{\alpha\beta})$	−0.37	−0.32	−0.26	−0.28
$f'_{d\beta}$	−0.10	0.15	−0.02	E″ species:				
$f'_{\beta\beta}$	0.13	−0.22	−0.06	$F_{88} = f_\beta - f_{\beta\beta} - f'_{\beta\beta} - f''_{\beta\beta}$	1.40	1.14	0.85	1.14
$f'_{\alpha\beta}$	−0.09	−0.01	0.005					

	$ClO_3F_2^-$		$BrO_3F_2^-$		XeO_3F_2		OsO_3F_2	
assgnt	DFT freq[d,f]	PED (B-matrix)[g]	DFT freq[d,f]	PED (B-matrix)[g]	DFT freq[d,f]	PED (B-matrix)[g]	DFT freq[d,f]	PED (B-matrix)[g]
$\nu_1(A_1')$	862	100 S_1	787	100 S_1	761	100 S_1	965	99 S_1 + 1 S_2
$\nu_2(A_1')$	383	100 S_2	430	100 S_2	510	100 S_2	617	99 S_2 + 1 S_1
$\nu_3(A_2'')$	622	77 S_3 + 23 S_4	529	80 S_3 + 20 S_4	595	93 S_3 + 7 S_4	655	100 S_3
$\nu_4(A_2'')$	474	1 S_3 + 99 S_4	423	4 S_3 + 96 S_4	326	1 S_3 + 99 S_4	262	2 S_3 + 98 S_4
$\nu_5(E')$	1133	12 $S_{5/6}$ + 57 $S_{6/5}$ + 22 $S_{7/8}$ + 8 $S_{9/10}$	886	76 $S_{5/6}$ + 13 $S_{6/5}$ + 5 $S_{7/8}$ + 3 $S_{8/7}$ + 2 $S_{9/10}$ + 1 $S_{10/9}$	845	93 $S_{5/6}$ + 3 $S_{6/5}$ + 3 $S_{8/7}$ + 1 $S_{10/9}$	957	21 $S_{5/6}$ + 76 $S_{6/5}$ + 1 $S_{7/8}$ + 2 $S_{8/7}$
$\nu_6(E')$	484	1 $S_{5/6}$ + 85 $S_{8/7}$ + 14 $S_{10/9}$	357	3 $S_{7/8}$ + 77 $S_{8/7}$ + 20 $S_{10/9}$	276	74 $S_{8/7}$ + 26 $S_{10/9}$	312	85 $S_{8/7}$ + 15 $S_{10/9}$
$\nu_7(E')$	235	51 $S_{8/7}$ + 49 $S_{10/9}$	193	64 $S_{8/7}$ + 36 $S_{10/9}$	157	71 $S_{8/7}$ + 29 $S_{10/9}$	189	51 $S_{8/7}$ + 49 $S_{10/9}$
$\nu_8(E'')$	435	100 $S_{11/12}$	362	100 $S_{11/12}$	291	100 $S_{11/12}$	353	99 $S_{11/12}$ + 1 $S_{12/11}$

[a] The internal force constants corresponding to E−O and E−F stretching are denoted by f_D and f_d, respectively, and the O−E−O and O−E−F bends are denoted by f_α and f_β, respectively. The interaction force constants are denoted by f_{xx}, f_{xy}, f'_{xx}, and f'_{xy}, where x and y are D, d, α, or β. The relative contributions of the internal coordinates to the PED of a normal coordinate are multiplied by 100. [b] Force constants for bond stretches and bends are given in mdyne Å^{-1} and mdyne Å rad^{-2}, respectively. [c] The force constants, F_{ii} ($i = 1\cdots8$), correspond to the normal modes, ν_i. The symmetry force constants F_{ij} correspond to the off-diagonal interactions between ν_i and ν_j, where $i \neq j$. [d] Frequencies are given in cm^{-1}. [e] Frequencies calculated from the normal coordinate analysis. [f] The vibrational frequencies and second derivative matrix used for the determination of the symmetry force constants were calculated by use of the SVWN method in conjunction with DZVP basis sets. When constrained to D_{3h} symmetry, the energy-minimized E−F and E−O bond lengths were $BrO_3F_2^-$ (1.916, 1.646 Å), XeO_3F_2 (1.983, 1.802 Å), OsO_3F_2 (1.897, 1.717 Å), and $ClO_3F_2^-$ (1.878, 1.477 Å), respectively. [g] The PEDs are given in percentages and have been normalized. The following symmetry coordinates were used and appear in the B-matrix potential energy distributions: S_1 = E−O1 + E−O2 + E−O3, S_2 = E−F1 + E−F2, S_3 = E−F1 − E−F2, S_4 = ∠O1EF1 + ∠O2EF1 + ∠O3EF1 − ∠O1EF2 − ∠O2EF2 − ∠O3EF2, S_5 = 2E−O1 − (E−O2 + E−O3), S_6 = E−O2 − E−O3, S_7 = 2∠O1EO3 − (∠O3EO2 + ∠O1EO2), S_8 = ∠O3EO2 − ∠O1EO2, S_9 = 2(∠O2EF1 + ∠O2EF2) − (∠O1EF1 + ∠O3EF1 + ∠O1EF2 + ∠O3EF2), S_{10} = ∠O1EF1 + ∠O1EF2 − ∠O3EF2 − ∠O3EF2, S_{11} = 2(∠O2EF1 − ∠O2EF2) − ∠O1EF1 + ∠O1EF2 − ∠O3EF1 + ∠O3EF2, S_{12} = ∠O1EF1 − ∠O1EF2 − ∠O3EF1 + ∠O3EF2. Their explicit forms are given in refs 72 and 77.

The O−E−F bending force constants, f_β, of $BrO_3F_2^-$, XeO_3F_2, and OsO_3F_2 are large relative to the O−E−O bending force constants, f_α. The repulsive interligand O···F interactions in these species may account, in part, for the greater magnitudes of these force constants, but the observation that f_β is greater for XeO_3F_2 than for OsO_3F_2, despite the shorter bond lengths and ligand−ligand distances calculated for OsO_3F_2, implies that other factors are involved. The decrease in f_β with increasing principal quantum number of the central element over the series suggests that the trend may be related to valence orbital diffuseness. A similar, but less pronounced, trend occurs among the O−E−O bending force constants of $BrO_3F_2^-$, XeO_3F_2, and OsO_3F_2, whose overall lower values are attributed to the large O−E−O bond angles (120°) that result in decreased interligand O···O interactions.

(ii) Symmetry Force Constants Derived from B-Matrix Analyses. The unscaled symmetry force constants and potential energy distributions of $BrO_3F_2^-$, XeO_3F_2, OsO_3F_2, and the unknown $ClO_3F_2^-$ anion determined by the B-matrix method are listed in Table 4. The relationships between the symmetry coordinates and internal coordinates of these systems are given in refs 72 and 77, and descriptions of the symmetry coordinates are provided in Table 4 (footnote g). The relationships between the symmetry force constants and the internal force constants of trigonal bipyramidal EY_3Z_2-type molecules have been derived previously[72] and are also provided in Table 4. A full comparison of the force constants obtained by the two methods is not possible because the FG-matrix method does not properly address all of the off-diagonal terms, which are arbitrarily set equal to zero. The values of diagonal terms (F_{11}/F_{55} and f_D; F_{22}/F_{33} and f_d, F_{66} and f_α; F_{77}/F_{88} and f_β) for $BrO_3F_2^-$, XeO_3F_2, and OsO_3F_2 are in general agreement, which is consistent with the relatively small values of the internal interaction force constants in the expressions for symmetry force constants.

The potential energy distributions determined from the B-matrix analyses of $ClO_3F_2^-$, $BrO_3F_2^-$, XeO_3F_2, and OsO_3F_2 (Table 4) reveal that there is no mixing of the symmetry coordinates for the A_1' modes. Among the A_2'' modes,

significant mixing only occurs between the asymmetric EF_2 stretches, S_3, and the out-of-plane umbrella bends, S_4, of $\nu_3(A_2'')$ in $ClO_3F_2^-$ and $BrO_3F_2^-$. The three E′ modes have contributions from S_5-S_{10}, with the degree of coupling being least for $\nu_5(E')$. The $\nu_5(E')$ mode is best described in terms of the degenerate EO_3 stretching symmetry coordinates, $S_{5/6}$, for $BrO_3F_2^-$, XeO_3F_2, and OsO_3F_2. In the case of $ClO_3F_2^-$, they are extensively mixed with the EO_3 bending symmetry coordinates, $S_{7/8}$. In contrast, $\nu_6(E')$ and $\nu_7(E')$ exhibit extensive mixing among their EOF bending coordinates, $S_{7/8}$ and $S_{9/10}$, but little or no mixing with the $S_{5/6}$ stretching coordinates.

Although the E−O bonds of XeO_3F_2 are expected to be less polar than those of $BrO_3F_2^-$, their symmetric (F_{11}) and antisymmetric (F_{55}) EO_3 stretching force constants are similar. This may, in part, arise from the greater underestimation of the EO_3 stretching frequencies (average $\nu_{expt} - \nu_{calcd}$ values for $\nu_1(A_1')$ and $\nu_4(A_2'')$ are given in parentheses) of XeO_3F_2 (49 cm^{-1}) relative to those of $BrO_3F_2^-$ (12 cm^{-1}). The main-group F_{11} and F_{55} values contrast with significantly higher values for OsO_3F_2, which may be attributed to stronger Os−O bonds arising from $d\pi-p\pi$ bonding contributions, as already noted for the internal force constants. Comparisons of the EO_3 stretching force constants of $BrO_3F_2^-$ with those of $ClO_3F_2^-$ reveal that F_{11} and F_{55} are 1.15 and 1.33 mdyne $Å^{-1}$ higher, respectively, for $ClO_3F_2^-$, in accord with the calculated Cl−O bond order of $ClO_3F_2^-$, which is 7% greater than the Br−O bond order of $BrO_3F_2^-$ (Table S6) and the weaker fluoride ion acceptor properties of ClO_3F. The value of F_{11} is similar to that of F_{55} for $ClO_3F_2^-$, $BrO_3F_2^-$, and XeO_3F_2, but it is significantly greater than F_{55} for OsO_3F_2, accounting for the occurrence of the symmetric OsO_3 stretch, $\nu_1(A_1')$, at higher frequency than the antisymmetric OsO_3 stretch, $\nu_5(E')$.[31]

The internal force constant, f_d, dominates the expressions for the symmetric (F_{22}) and antisymmetric (F_{33}) EF_2 symmetry force constants, accounting for similar trends among the internal and symmetry force constants associated with the symmetric and antisymmetric EF_2 stretches. The symmetric EF_2 stretching symmetry force constant is greater than its antisymmetric counterpart for OsO_3F_2 (4.30, 4.13 mdyne $Å^{-1}$), XeO_3F_2 (2.92, 3.04 mdyne $Å^{-1}$), and $BrO_3F_2^-$ (2.09, 2.19 mdyne $Å^{-1}$), with the order reversed at $ClO_3F_2^-$ (1.68, 1.73 mdyne $Å^{-1}$). The orderings cannot, however, be accounted for in terms of the f_{dd} contributions to F_{22} and F_{33} derived from experimental frequencies. The higher symmetry force constants of the symmetric and antisymmetric BrF_2 stretches of $BrO_3F_2^-$ relative to those of $ClO_3F_2^-$ are in accord with the greater fluoride ion basicity of $ClO_3F_2^-$ and with the Br−F bond order of $BrO_3F_2^-$, which is 45% greater than the Cl−F bond order of $ClO_3F_2^-$ (vide infra). Decreases in F_{44} along the series $ClO_3F_2^- > BrO_3F_2^- > XeO_3F_2 > OsO_3F_2$ reflect decreasing resistance to angular distortions for the out-of-plane EO_3 bend with increasing size of the central atom, with F_{77} and F_{88} of the in-plane EO_2 bends showing similar, but less pronounced, trends.

(e) Atomic Charges and Bond Orders. The atomic charges, valencies, and bond orders of XO_4^-, XO_3F, and $XO_3F_2^-$ (X = Cl, Br) are provided in Table S6 and were calculated by use of the natural bond orbital (NBO) method in conjunction with the energy-minimized geometries determined by the LDF (MPW1PW91) method.

The positive charges on the bromine (2.71−2.78) and chlorine (2.43−2.49) atoms exhibit little variation among the oxygen-rich species XO_4^-, XO_3F, and $XO_3F_2^-$ (X = Br, Cl) and are similar to those reported for BrF_6^+ (2.86) and ClF_6^+ (2.51) using the same computational method.[51] The positive charges on the chlorine atoms are approximately 0.3 less than those on the bromine atoms of their bromine analogues and are attributed to the higher electronegativity of chlorine. The relative invariance of the central halogen atom charge requires that the atomic charges on the oxygen and fluorine ligands compensate the net charges of these species. The negative charge distributions among the oxygen and fluorine ligands of XO_3F (82/82% O, 18/18% F) and $XO_3F_2^-$ (63/67% O, 38/33% F) are similar for X = Cl and Br, with the negative charge distribution shifting toward the fluorine atoms in the anions, in accord with the enhanced polarities and lower bond orders of the X−F bonds (vide infra). A comparison of the calculated X−F bond orders of XO_3F and $XO_3F_2^-$ shows that they correlate with the relative fluoride ion affinities of BrO_3F and ClO_3F, with a Br−F bond order for $BrO_3F_2^-$ that is 73% of that calculated for BrO_3F and a Cl−F bond order for $ClO_3F_2^-$ that is only 58% of that calculated for ClO_3F. Although the calculated Cl−O bond orders are slightly higher (ca. 5%), the X−O bond orders show the same ordering and little variation for each pair of analogues, XO_4^-, XO_3F, and $XO_3F_2^-$. Similar trends are found among the ligand valencies of these species (Table S6).

Conclusion

Perbromyl fluoride is a sufficiently strong fluoride ion acceptor toward MF (M = K, Rb, Cs, $N(CH_3)_4$), and NOF to form stable salts of the $BrO_3F_2^-$ anion. With the exception of $[NO]_2[BrO_3F_2][F]$, which has a significant dissociation vapor pressure, the $BrO_3F_2^-$ salts studied are all stable under dynamic vacuum at −40 °C, and β-$[Cs][BrO_3F_2]$ can be handled for up to several hours under inert conditions at ambient temperatures. The fully assigned vibrational spectra of the aforementioned salts and X-ray crystal structures of $[NO]_2[BrO_3F_2][F]$ and $[N(CH_3)_4][BrO_3F_2]$ establish the trigonal bipyramidal geometry of $BrO_3F_2^-$ predicted by the VSEPR model of molecular geometry. The $BrO_3F_2^-$ anion is only the fourth Br(VII) species to have been isolated in macroscopic quantities and structurally characterized and is one of only three oxide fluorides known to possess D_{3h} symmetry, the others being XeO_3F_2 and matrix-isolated OsO_3F_2 monomer.

The $BrO_3F_2^-$ salts described in this work provide experimental confirmation of the fluoride ion affinity of BrO_3F calculated in this and in previous work.[26] Attempts to prepare salts containing the $ClO_3F_2^-$ and $BrO_3F_3^{2-}$ anions by the reactions of ClO_3F and $[N(CH_3)_4][BrO_3F_2]$ with $[N(CH_3)_4][F]$ were unsuccessful. Gas-phase electronic structure calculations confirm that the *fac*- and *mer*-isomers of the $BrO_3F_3^{2-}$ dianion are unstable, whereas $ClO_3F_2^-$ and $BrO_3F_2^-$ are predicted to be thermodynamically stable with respect to fluoride ion loss. The enthalpy of fluoride ion attachment for ClO_3F (−132 kJ mol^{-1}) is, however, considerably less exothermic than that of BrO_3F (−261 kJ mol^{-1}) and is comparable with the minimum value typically required for the formation of a stable anion (−126 to −146 kJ mol^{-1}) when lattice and solvation energies are taken into account.[26] The calculated $BrO_3F_2^-$ and $ClO_3F_2^-$ bond orders indicate that the X−O bonds of $ClO_3F_2^-$ are stronger but the X−F bonds of $ClO_3F_2^-$ are weaker than those

of $BrO_3F_2^-$, which is consistent with the internal and symmetry force constant analyses of these anions and the greater fluoride ion affinity of BrO_3F relative to that of ClO_3F.

Experimental Section

Caution: Anhydrous HF must be handled using appropriate protective gear with immediate access to proper treatment procedures[78−80] in the event of contact with liquid HF, HF vapor, or HF-containing solutions. Perbromyl fluoride, ClO_3F, and the $BrO_3F_2^-$ salts are strong oxidants and may react vigorously to explosively with water, organic compounds, and other oxidizable materials. The syntheses of $[M][BrO_3F_2]$ ($M = K$, Rb, Cs, $N(CH_3)_4$) are specifically cautioned, as solutions of BrO_3F and CH_3CN have, on occasion, detonated. Small-scale (<100 mg) syntheses of the aforementioned salts are recommended.

(a) Apparatus and Materials. All volatile materials were handled in vacuum lines constructed of stainless steel, nickel, and FEP fluoroplastic, whereas nonvolatile materials were transferred in a drybox as previously described.[81] Acetonitrile (Caledon, HPLC grade) was purified by the literature method[82] and transferred under static vacuum on a glass vacuum line. Potassium perbromate,[7] AsF_5,[83] NOF,[84] and anhydrous $[N(CH_3)_4][F]$[37] were prepared and purified according to literature methods. Sodium fluoride (J. T. Baker Chemical Co., 99%) and KF (J. T. Baker Chemical, 99%) were dried in a glass vessel under dynamic vacuum at 250−300 °C for a minimum of 3 days and stored in a drybox. Cesium fluoride (Aldrich, 99.9%) and RbF (ICN-K&K Laboratories Inc., 99.9%) were dried by fusion in a platinum crucible, and the molten salts were allowed to cool under dynamic vacuum in the antechamber of a drybox. The resulting CsF and RbF pellets were ground inside a drybox and stored in PFA or FEP vessels. Anhydrous HF was purified as previously described[39] and stored over BiF_5 in a Kel-F vessel. High-purity Ar or N_2 gases were used for backfilling vessels.

BrO_3F. Perbromyl fluoride was prepared as previously described[1,24] by the reaction of AsF_5 with $[K][BrO_4]$ in anhydrous HF at ambient temperature. In a typical reaction, 110 mg (0.601 mmol) of $[K][BrO_4]$ was dissolved in 0.75 mL of HF in a $^1/_4$-in. o.d. FEP vessel equipped with a Kel-F valve. Arsenic pentafluoride (0.306 g, 1.80 mmol) was then condensed into the vessel at −196 °C, and the vessel was backfilled with Ar after dissolution of the AsF_5 in HF at −78 °C. The vessel and contents were warmed to ambient temperature for 45−60 min with periodic mixing to ensure complete reaction. The solution was again cooled to −78 °C, and the volatile components were distilled under dynamic vacuum into a 5/8-in. o.d. FEP U-tube (−196 °C) containing 3 g of dry NaF. The U-tube and contents were isolated under static vacuum and warmed to ambient temperature using a water bath, which served as a heat sink for the exothermic reactions of HF and AsF_5 with NaF. After 5−10 min, the U-tube was cooled to −196 °C, and the vacuum in the tube was refreshed. Purified BrO_3F was transferred by rapidly warming the U-tube to ambient temperature using a water bath and condensing the volatile product under static vacuum into a $^1/_4$-in. or 4-mm o.d. FEP reaction vessel at −196 °C.

$[M][BrO_3F_2]$ ($M = K$, Rb, Cs, $N(CH_3)_4$). The title salts were prepared by reaction of BrO_3F with the alkali metal fluorides and $[N(CH_3)_4][F]$ in CH_3CN. The formation of the $BrO_3F_2^-$ salt and consumption of BrO_3F were monitored by periodically freezing the reaction mixtures and recording their Raman spectra at −163 °C. In the case of $[Rb][BrO_3F_2]$, the progress of the reaction was also followed by monitoring the intensities of the strong RbF bands at 3144(100), 3160(87), 3338(4), 3357(2), and 3396(21) cm^{-1}. Typically, CH_3CN solvent (0.25 mL) was condensed into a 4-mm or $^1/_4$-in. o.d. FEP vessel containing 0.1 to 0.2 mmol of powdered MF ($M = Cs$, Rb, K, $N(CH_3)_4$). The vessel was backfilled with N_2 and temporarily stored at −78 °C to prevent the alkali metal fluorides and, in particular, $[N(CH_3)_4][F]$[37,38] from reacting with the solvent. A stoichiometric excess of BrO_3F (ca. 0.6 mmol) was condensed into the vessel at −196 °C (vide supra), and the vessel was backfilled with 1000 Torr of Ar at −78 °C. The mixture was warmed to above the melting point of the CH_3CN solvent for 1 h prior to isolation of the colorless salts by removal of the solvent and excess BrO_3F under dynamic vacuum at this temperature. The optimum reaction temperature varied from salt to salt, likely reflecting the relative solubilities of the fluoride ion donors. Cesium fluoride readily reacted with BrO_3F in CH_3CN at −40 to −48 °C to produce α-$[Cs][BrO_3F_2]$, but formed β-$[Cs][BrO_3F_2]$ when the solution was warmed to −35 °C. The high-temperature β-phase was also prepared by warming α-$[Cs][BrO_3F_2]$ to 0 °C in the absence of a solvent while monitoring the phase transition by Raman spectroscopy. Complete conversion of α-$[Cs][BrO_3F_2]$ to β-$[Cs][BrO_3F_2]$ by the latter method required ca. 35 h. The reactions of KF and RbF with BrO_3F proceeded very slowly below −40 °C, but within an hour when warmed to between −30 and −35 °C. The reaction of $[N(CH_3)_4][F]$ with BrO_3F proceeded at −40 °C; however, warming these CH_3CN solutions above 0 °C led to slow reaction of $BrO_3F_2^-$ with CH_3CN to produce NO_2F (δ (^{19}F), 396.6 ppm; $^3J(^{19}F-^{14}N)$, 115 Hz), CH_3COF (δ (^{19}F), 49.0 ppm; $^3J(^{19}F-^1H)$, 7.2 Hz), and BrO_4^- (δ (^{79}Br), 2482 ppm).

$[NO]_2[BrO_3F_2][F]$. The salt, $[NO]_2[BrO_3F_2][F]$, was synthesized by the reaction of BrO_3F with liquid NOF at −78 °C. Perbromyl fluoride (ca. 0.6 mmol) was condensed into a $^1/_4$-in. o.d. FEP vessel containing 0.1 mL of NOF (ca. 0.13 g, 2.7 mmol) which, upon warming to −78 °C, resulted in a colorless solid. The vessel was briefly (ca. 30 s) evacuated at −78 °C until the last visible traces of the liquid reagents had evaporated, but was not pumped on further because the product has an appreciable dissociation vapor pressure and rapidly pumps off at −78 °C.

Attempted Syntheses of $[N(CH_3)_4]_2[BrO_3F_3]$ and $[N(CH_3)_4][ClO_3F_2]$. The synthesis of $[N(CH_3)_4]_2[BrO_3F_3]$ was attempted by addition of $[N(CH_3)_4][F]$ (6.98 mg, 74.9 μmol) to $[N(CH_3)_4][BrO_3F_2]$ (6.48 mg, 69.6 μmol) at −160 °C in a 4-mm o.d. FEP vessel. Acetonitrile (0.1 mL) was then condensed into the vessel, and the solution was warmed to 0 °C for 5 min to dissolve the reagents. The Raman spectrum of the colorless solid remaining after solvent removal under dynamic vacuum at −40 °C was a mixture of $[N(CH_3)_4][BrO_3F_2]$ and $[N(CH_3)_4)][F]$,[38] indicating that transfer of a second fluoride ion to BrO_3F to form $[N(CH_3)_4]_2[BrO_3F_3]$ had not occurred.

The synthesis of $[N(CH_3)_4][ClO_3F_2]$ was attempted by analogy with that of $[N(CH_3)_4][BrO_3F_2]$. Perchloryl fluoride (80.6 μmol, Pennsalt Chemicals) was condensed into an FEP vessel (4-mm o.d.) containing a preweighed amount of $[N(CH_3)_4][F]$ (7.51 mg, 80.6 μmol) dissolved in 0.3 mL of CH_3CN. The vessel was then warmed to −40 °C for 1 h with agitation before removal of the solvent at −40 °C under dynamic vacuum. The Raman spectrum of the remaining colorless solid, recorded at −40 °C, corresponded to that of $[N(CH_3)_4][F]$.[38] The synthesis of $[N(CH_3)_4][ClO_3F_2]$ was also attempted by the direct reaction of $[N(CH_3)_4][F]$ (28.5 mg; 0.306 mmol) with a large excess of ClO_3F (0.11 mL; 1.5 mmol) in a 4-mm o.d. FEP vessel. The reaction mixture was warmed to −40 °C for 2 h with periodic agitation. The Raman spectrum (−163 °C) of the colorless solid under ClO_3F was consistent with a mixture of $[N(CH_3)_4][F]$ and ClO_3F and provided no evidence for $[N(CH_3)_4][ClO_3F_2]$ formation. The Raman spectrum (−163 °C) of the solid remaining after the removal of the ClO_3F at −120 °C was that of $[N(CH_3)_4][F]$.

(b) X-ray Crystallography. (i) Crystal Growth. Crystals of $[N(CH_3)_4][BrO_3F_2]$ were grown as previously described[49] by slowly cooling a CH_3CN solution of the salt from 10 to −25 °C in a T-shaped

(77) Levin, I. W. *J. Mol. Spectrosc.* **1970**, *33*, 61.
(78) Bertolini, J. C. *J. Emerg. Med.* **1992**, *10*, 163.
(79) Peters, D.; Miethchen, R. *J. Fluorine Chem.* **1996**, *79*, 161.
(80) Segal, E. B. *Chem. Health Saf.* **2000**, 19.
(81) Casteel, W. J., Jr.; Kolb, P.; LeBlond, N.; Mercier, H. P. A.; Schrobilgen, G. J. *Inorg. Chem.* **1996**, *35*, 929.
(82) Winfield, J. M. *J. Fluorine Chem.* **1984**, *25*, 91.
(83) Mercier, H. P. A.; Sanders, J. C. P.; Schrobilgen, G. J.; Tsai, S. S. *Inorg. Chem.* **1993**, *32*, 386.
(84) Christe, K. O. *Inorg. Chem.* **1973**, *12*, 1580.

$^1/_4$-in. o.d. FEP vessel. After crystal growth was complete, the solvent was decanted into the sidearm of the T-reactor and cooled to −196 °C, and the sidearm was heat-sealed off and removed under dynamic vacuum. The colorless, tetragonal-shaped crystals were dried under dynamic vacuum at −40 °C and stored at −78 °C until mounted on the diffractometer. Crystals of $[NO]_2[BrO_3F_2][F]$ were grown by sublimation of the initial product under 1000 Torr of Ar in a $^1/_4$-in. FEP vessel over the course of several weeks while stored in a dewar filled with solid dry ice. The colorless, block-shaped crystals accumulated in the cooler upper region of the vessel where fresh dry ice had been added daily.

(ii) Crystal Mounting and Data Collection. A single crystal of $[N(CH_3)_4][BrO_3F_2]$ was mounted on a glass fiber at −110 ± 5 °C using a Fomblin oil as an adhesive.[85] A crystal of $[NO]_2[BrO_3F_2][F]$ was mounted in a similar fashion; however, the substantial dissociation vapor pressure of this salt and its tendency to sublime in a cold stream of dry N_2 at −110 °C required that it be mounted at −150 °C.

Mounted crystals were centered on a P4 Siemens diffractometer (−173 °C) equipped with a Siemens SMART 1K CCD area detector, a rotating molybdenum anode ($\lambda_K \alpha = 0.71073$ Å, monochromated by a graphite crystal) and controlled by SMART.[86] The distance between the crystal and the detector face was 4.970 ($[NO]_2[BrO_3F_2][F]$) or 4.987 cm ($[N(CH_3)_4][BrO_3F_2]$), and the data sets were collected in 512 × 512 pixel mode using 2 × 2 pixel binning. The raw diffraction data sets were integrated and scaled as previously described[49] using SAINT+[87] and SADABS.[88]

(iii) Solution and Refinement. The program XPREP[89] was used to confirm unit cell dimensions and space groups. Direct methods were used to locate the bromine atoms, and the lighter atom positions were identified in successive difference Fourier syntheses. Final refinements were obtained using data that had been corrected for absorption by introducing an extinction coefficient and were optimized using anisotropic thermal parameters for all atoms except the hydrogen atoms of the $N(CH_3)_4^+$ cation. Attempts to constrain the bond angles and/or bond lengths of the anion in the disordered structure of $[N(CH_3)_4][BrO_3F_2]$ did not improve the global solution and therefore were not utilized in the final refinement of the structure.

(c) NMR Spectroscopy. The solution ^{19}F (470.592 MHz), ^1H (500.130 MHz), and ^{13}C (125.758 MHz) spectra of $[N(CH_3)_4][BrO_3F_2]$ in CH_3CN solvent at −40 °C were recorded on a Bruker DRX-500 (11.7438 T) spectrometer operating in unlocked mode (field drift < 0.1 Hz h^{-1}) using a 5-mm $^1H/^{13}C/^{19}F/^{31}P$ QNP probe. The spectra were externally referenced to neat $CFCl_3$ (^{19}F) and $Si(CH_3)_4$ (^1H, ^{13}C) at 27 °C. The following acquisition parameters were used: pulse widths 2.3 (^{19}F), 7.7 (^1H), 12.8 (^{13}C) μs; acquisition times 0.174 (^{19}F), 2.42 (^1H), 0.565 (^{13}C) s; spectral widths 18.8 (^{19}F), 6.8 (^1H), 29.0 (^{13}C) kHz. Free induction decays were recorded in 32 K memories, zero filled to 64 K memories and Fourier transformed, resulting in data point resolutions of 2.9 (^{19}F), 0.21 (^1H), 0.88 (^{13}C) Hz/data point.

(d) Vibrational Spectroscopy. Raman spectra were recorded on a Bruker RFS 100 FT-Raman spectrometer at −163 °C using 1064-nm excitation as previously described.[85] The infrared spectrum of β-$[Cs][BrO_3F_2]$ was recorded on a Bio-Rad FTS-40 spectrometer at ambient temperature. The three-layered AgCl pellet of $[Cs][BrO_3F_2]$ was fabricated in a drybox by use of a Wilks mini-press, with the external layers being composed of AgCl and the central layer being a mixture of the sample and AgCl.

(e) Calculations. The energy-minimized gas-phase structures, vibrational frequencies, atomic charges, Mayer bond orders, and valencies were calculated by use of the HF, MP2, and LDF (MPW1PW91) methods using Gaussian 98.[90] The 6-311G(d) (HF, MP2) and DZVP (MPW1PW91) basis sets were used in each case. The enthalpies of fluoride ion attachment to ClO_3F, BrO_3F, and $BrO_3F_2^-$ were calculated by use of the Gaussian-2 (G2) method.

The internal force constants of $BrO_3F_2^-$, XeO_3F_2, and OsO_3F_2 were determined by the Wilson FG-matrix method[74] using the software package SVIB.[91] The experimental geometry was used for $BrO_3F_2^-$, and the calculated LDF (MPW1PW91) values were used for XeO_3F_2 and OsO_3F_2 monomer. The symmetry force constants of $BrO_3F_2^-$, $ClO_3F_2^-$, XeO_3F_2, and OsO_3F_2 were determined by use of the B-matrix method using the second derivative potential energy matrixes obtained from their calculated structures (SVWN/DZVP) and the software package B-matrix.[75]

Acknowledgment. We thank the donors of the Petroleum Research Fund, administered by the American Chemical Society, for support of this work under ACS-PRF No. 37128-AC3 (G.J.S.), and the Natural Sciences and Engineering Research Council of Canada for a postgraduate scholarship and McMaster University for a Dalley Fellowship (J.F.L.). We are grateful to Prof. David A. Dixon for his assistance with the use of the B-matrix software package and to Dr. Hélène P. A. Mercier for her considerable assistance in preparing and critiquing this manuscript.

Supporting Information Available: Calculated vibrational frequencies of $BrO_3F_2^-$ and $ClO_3F_2^-$; stretching frequency trends among $BrO_3F_2^-$ salts; factor-group analysis of the $BrO_3F_2^-$ anion in $[NO]_2[BrO_3F_2][F]$; calculated geometries of *fac*-$BrO_3F_3^{2-}$ and *mer*-$BrO_3F_3^{2-}$ and enthalpies of fluoride ion attachment to $BrO_3F_2^-$ (complementary discussion); calculated vibrational frequencies and intensities for the $BrO_3F_2^-$ and $ClO_3F_2^-$ anions (Table S1); factor-group analysis of the $BrO_3F_2^-$ anion in $[NO]_2[BrO_3F_2][F]$ (Table S2); calculated geometric parameters of $BrO_3F_2^-$, $ClO_3F_2^-$, and $BrO_3F_3^{2-}$ (Table S3); calculated gas-phase enthalpies of fluoride ion attachment (Table S4); potential energy distributions for $BrO_3F_2^-$, XeO_3F_2, and OsO_3F_2 derived from GVFF analyses (Table S5); the disordered structure of $[N(CH_3)_4][BrO_3F_2]$ (Figure S1); displacement vectors for the fundamental vibrational modes of the $BrO_3F_2^-$ anion (Figure S2); and X-ray crystallographic files (CIF format) for the structure determinations of $[NO]_2[BrO_3F_2][F]$ and $[N(CH_3)_4][BrO_3F_2]$. This material is available free of charge via the Internet at http://pubs.acs.org.

JA0402607

(85) Gerken, M.; Dixon, D. A.; Schrobilgen, G. J. *Inorg. Chem.* **2000**, *39*, 4244.
(86) *SMART*, version 5.611; Siemens Energy and Automotive Analytical Instrumentation: Madison, WI, 1999.
(87) *SAINT+*, version 6.02; Siemens Energy and Automotive Analytical Instrumentation: Madison, WI, 1999.
(88) Sheldrick, G. M. *SADABS* (Siemens Area Detector Absorption Corrections), version 2.03; Bruker AXS, Inc.: Madison, WI, 1999.
(89) Sheldrick, G. M. *SHELXTL*, version 5.1; Siemens Analytical X-ray Instruments, Inc.: Madison, WI, 1998.
(90) Frisch, M. J.; Trucks, G. W.; Schlegel, H. B.; Scuseria, G. E.; Robb, M. A.; Cheeseman, J. R.; Zakrzewski, V. G.; Montgomery, J. A., Jr.; Stratmann, R. E.; Burant, J. C.; Dapprich, S.; Millam, J. M.; Daniels, A. D.; Kudin, K. N.; Strain, M. C.; Farkas, O.; Tomasi, J.; Barone, V.; Cossi, M.; Cammi, R.; Mennucci, B.; Pomelli, C.; Adamo, C.; Clifford, S.; Ochterski, J.; Petersson, G. A.; Ayala, P. Y.; Cui, Q.; Morokuma, K.; Salvador, P.; Dannenberg, J. J.; Malick D. K.; Rabuck, A. D.; Raghavachari, K.; Foresman, J. B.; Ciosloski, J.; Ortiz, J. V.; Baboul, A. G.; Stefanov, B. B.; Lui, G.; Liashenko, A.; Piskorz, P.; Komaromi, I.; Gomperts, R.; Martin, R. L.; Fox, D. J.; Keith, T.; Al-Laham, M. A.; Peng, C. Y.; Nanayakkara, A.; Gonzalez, C.; Challacombe, M.; Gill, P. M. W.; Johnson, B.; Chen, W.; Wong, M. W.; Andres, J. L.; Gonzalez, C.; Head-Gordon, M.; Replogle, E. S.; Pople, J. A. *Gaussian 98*, revision A.11; Gaussian, Inc.: Pittsburgh, PA, 2001.
(91) Mukherjee, A.; Spiro, T. G. SVIB Program, An Expert System for Vibrational Analysis; Program 656, Bulletin 15(1); Quantum Chemistry Program Exchange: Indiana University, 1995.